Nonlinear vibration mitigation of a rotor-casing system subjected to imbalance-looseness-rub coupled fault

Yang Yang[1*], Guo Chen[2], Huajiang Ouyang[3], Yiren Yang[1], Dengqing Cao[4]

1. School of Mechanics and Engineering, Southwest Jiaotong University, Chengdu 610031, China

2. National Key Laboratory of Science and Technology on Reactor System Design Technology, Nuclear Power Institute of China, Chengdu 610213, China

3. Centre for Engineering Dynamics, School Engineering, University of Liverpool, Liverpool L69 3GH, UK

4. School of Astronautics, Harbin Institute of Technology, PO Box 137, Harbin 150001, China

Abstract: Modern industrial requirements are continuously demanding better performances and higher rotational speeds from current aero-engines. Under this circumstance, mitigation of rotor vibration is of considerable importance for safe and efficient functioning of rotating machinery. The main objective of this paper is to investigate the application of nonlinear vibration absorber on vibration suppression of a rotor-casing system having imbalance-looseness-rub coupled fault. Due to large vibration amplitude and pedestal looseness, both the geometrical nonlinearity of the rotor shaft and the support nonlinearity are considered in the system. When dealing with blade-casing rub, the initial gap between them is treated to be in non-uniform distribution because of coating inhomogeneity. Then the equations of motion in the presence and absence of nonlinear vibration absorber are respectively obtained according to the Lagrange's equation. Through numerical simulation, the vibration mitigation of the rotor-casing system is realized in the different conditions of rotational speed and disc eccentricity. Moreover, from the perspective of vibration displacement and impact force, the effects of the nonlinear vibration absorber on the pedestal looseness and blade-casing rub are further discussed. The numerical results reveal that the nonlinear vibration absorber can effectively suppress the nonlinear vibration of the system and alleviate the detrimental influence of the coupled fault in a wide frequency range.

Key words: rotor-casing system, imbalance-looseness-rub coupled fault, vibration mitigation, nonlinear vibration absorber.

1. Introduction

Rotating machines, such as generator sets, aero-engines and wind turbines, play a significant pole in modern industry. Hence, the in-depth and comprehensive research on the behaviour of rotating machinery and the associated phenomena become extremely relevant [1-3]. Due to the increase of rotational speed and the narrowing of initial rotor-stator gap, the possible contact between rotor and stator is considered a serious malfunction that may lead to catastrophic failure [4-6]. In order to achieve condition monitoring and appropriate design of rotating machinery, it is of high significance to analyse their dynamic performance associated with rotor-stator rub fault.

*Corresponding author: Yang Yang, 181042yy@163.com; Guo Chen, apple88125@hotmail.com; Huajiang Ouyang, h.ouyang@liverpool.ac.uk; Yiren Yang, yangyiren05@126.com; Dengqing Cao, dqcao@hit.edu.cn;

As one of frequently-occurring faults in rotating machines, rub-impact fault has attracted a huge amount of interest all along. From the viewpoint of rotor-stator contact area, there are three types of rub-impact fault, including no rub, partial one and full annular one [7-10]. A full annular rub indicates that the rotor is in continuous contact with the stator, which usually happens under large unbalance. In contrast, a partial rub refers to intermittent rotor-stator rub, which is the most common in the rotating machinery. Up to now, many studies have been carried on the different types of rub-impact fault. Dai et al. [11] numerically investigated the forced nonlinear vibration of a rotor system subjected to full annular rub and motion-limiting stops. Zhang et al. [12] analytically studied the nonlinear synchronous full annular rub motion of a flexible rotor induced by the mass unbalance and the contact-rub force. Yu [13] discussed the reverse full annular rub based on a two degree-of-freedom rotor/seal model where a rubbing location could be simulated away from the lumped rotor mass. By utilizing an experimental apparatus, Choi [14] studied the dynamic behaviour of a rotor system with full annular rub. And then they observed that the phenomena of backward rolling and backward slipping were closely related to the friction and the eccentricity of the rotor. Vlajic et al. [15, 16] investigated the dynamics of a modified Jeffcott rotor that undergoes either forward synchronous whirling or self-excited backward whirling motions with continuous stator contact.

In order to detect and mitigate slight rub prior to more severe full rub condition, partial rub should be investigated in-depth. Smyth et al. [17] considered viscoelasticity in the stator support and investigated its influence on the global dynamics of rotor-stator rub, where the viscoelastic stator supports were modelled using fractional calculus. In reference [18], an overhung rotor model having two degrees of freedom was explored to determine the effect of friction during contact between rotor and stator. Pennacchi et al. [19] presented some experimental results obtained on a test rig, in which rub conditions of real machines were reproduced and short arc rub was considered. Torkhani et al. [20] built a numerical model and an experimental set-up to investigate the partial rub of a rotor in contact with a non-rotating obstacle. In particular, the dynamic behaviours corresponding to light, medium and severe partial rub were analysed in [20]. In order to study the stability and nonlinear dynamics of a complex braking system with a rotor-stator contact, Sinou et al. [21] developed a nonlinear strategy based on the centre manifold, the rational approximants and the alternating frequency/time domain method. In simulating rub-impact between the journal and the associated pads, Ebrahim et al. [22] employed mixed lubrication theory along with elastic-plastic asperity contact model. According to a modular kit, Ehehalt et al. [23] presented an integral experimental approach and then observed a great variety of vibration phenomena. Qin and Chen et al. [24-26] established a cylindrical shell model with arbitrary boundary conditions and simulated the partial rub between the rotating shell and stator in a rotor system.

Rotor-stator rub is usually identified as a secondary fault, which may be caused by mass imbalance, shaft crack, shaft misalignment and support looseness. It is worth noting that, due to manufacturing error, poor installation quality, long-term load, thermal effect and other factors, looseness fault has become one of the most common faults in rotary engines. To reduce vibration and noise and maintain the performance of rotating machinery, research on looseness fault has become a

popular topic [27]. Jiang et al. [28] proposed a nonlinearity measure based assessment method for the pedestal looseness of a rotor-bearing system under constant rotational speeds. Taking a simple drum rotor with bolted joints as an example, Qin et al. [29] calculated the influences of the time-varying joint stiffness resulting from the bolt loosening on the steady-state response of the rotor system. In [30], the self-loosening of bolts in curvic coupling was analysed by the self-rotation of nut in the cases of cyclic torque loads on discs after the preload of bolts. Muszynska et al. [31] studied the dynamic behaviour of a one-lateral-mode unbalanced and radially side-loaded rotor with either a loose pedestal, or with occasional rotor-to-stator rubbing. The above literature indicates that the existence of rub-impact and looseness will indeed lead to vibration with large amplitude, reduce operation quality, and even cause some disastrous consequences.

As far as the stability and safety of the rotating machinery are concerned, how to make noise reduction and suppress undesired vibration is one of the key problems to be solved urgently. Under this circumstance, these aims may be achieved by structural control [32]. According to the inherent characteristics of the control strategy, there are usually four main groups, including passive, semi-active, active, and hybrid methods. Active absorbers act on feedback to a control system, which could deal with multiple modes of vibration. Since it is difficult to install a large number of devices needed for active control in the limited internal space of rotating machinery, passive control methods are gradually accepted by the majority of researchers in recent decades. As described in [33], there are two commonly used passive devices for vibration reduction, namely the linear vibration absorber and the nonlinear vibration absorber. The linear vibration absorber usually refers to the linear tuned mass damper (TMD), which consists of a linear spring and a mass and sometimes a viscous damper. However, TMD only attenuates the vibration of a primary system over a relatively narrow frequency range [34]. The nonlinear vibration absorber as a bigger concept can be thought to contain three sub-types: a nonlinear tuned vibration absorber, a nonlinear energy sink, and a bistable tuned vibration absorber, according to whether the linear stiffness term is positive, vanishing, or negative [35, 36]. Through a nonlinear vibration absorber, the irreversible energy transfer from the primary system to the nonlinear attachment is activated [37]. There are two elements in a nonlinear vibration absorber: an essentially nonlinear stiffness and a linear viscous damper. Different from a linear TMD, a nonlinear vibration absorber is capable of efficient vibration mitigation over a relatively wide frequency range. In the past years, the vibration control of system by employing the nonlinear vibration absorber has attracted a huge amount of interest already. Gendelman et al. [38, 39] demonstrated the ability of a simple eccentric rotator to perform as a nonlinear vibration absorber in theoretical and experimental methods. Ahmadabadi [40] proposed an application of lightweight vibration control strategy known as nonlinear vibration absorber to mitigate the undesired vibrations in engine crankshaft systems. Parseh et al. [41] considered a nonlinear, simply supported beam under harmonic excitation coupled to a nonlinear vibration absorber. On this basis, they investigated the steady state dynamic of the beam by combing averaging method with arc-length continuation. Kani et al. [42] presented the analysis of the energy transfer between the nonlinear beam and the nonlinear vibration absorber, in which the control parameters were optimized by both sensitive analysis and particle swarm optimization. Bab et al. [43-45] installed a number of smooth nonlinear vibration

absorbers on the rotor-bearing system and performed a vibration attenuation analysis in an operating speed range. Tehrani et al. [46] studied the application of linear and nonlinear vibration absorbers on the vibration mitigation of a rotor system with several flexible blades. Additionally, they discussed the bifurcation diagrams and the Lyapunov exponent of the system under different parameters. In [47], the vibration reduction of a rotor system was investigated by employing different passive control methods.

Different from the previous analysis of dynamic phenomena and nonlinear mechanism in nonlinear mechanics, this paper focuses on suppressing or even eliminating the adverse effects of blade-casing rub and pedestal looseness through nonlinear vibration absorber. By analyzing the vertical vibration of the loose pedestal and the impact force of the blades, the response difference of the rotor-casing system induced by the nonlinear vibration absorber is investigated. This paper is organized as follows: Firstly, the governing equations of motion of the rotor-casing system without and with the nonlinear vibration absorber are respectively derived in Section 2. In this part, the blade-casing rub model in the presence of non-uniform gap and the pedestal looseness model are given. Secondly, the vibration characteristics of the system without nonlinear vibration absorber are studied in Section 3, in which the effects of geometrical nonlinearity of shaft and the support nonlinearity of loose pedestal are considered. After that, the vibration mitigation of the rotor-casing system having the above coupled fault is realized by the nonlinear vibration absorber in Section 4. At last, some conclusions are summarized in Section 5.

2. Governing equations of motion

In this section, considering the action of imbalance-pedestal looseness-rub coupled fault, the governing equations of motion of a rotor-casing system in the presence and absence of a nonlinear vibration absorber are respectively derived by using the Lagrange's equation. Fig. 1 depicts a rotor-casing system, which includes a casing, a continuous rotating shaft, a disc with an absorber, two pedestals and eight straight blades. In the dynamic model process, several assumptions are made as follows:

(1) The shaft is modelled as a massless flexible Euler beam with uniform circular cross section.

(2) The disc is considered as an annular rigid body having a mass eccentricity. At the same time, it is installed in the middle of the shaft.

(3) Because the stiffness of the blades installed in some rotor test rigs is much larger than that of the shaft, the elastic deformation of the blades is ignored. In addition, all the blades are identical, including material characteristic and geometrical dimension.

(4) The casing is treated as a lumped mass, which is supported by linear springs and viscous dampers.

(5) The impact between blades and casing happens in the normal direction. Meanwhile, the tangential rub between them is assumed to be a sliding friction.

(6) The thermal effects and friction torque caused by the rub-impact are not considered.

(7) The operating speed of the rotor system is higher than the first critical speed, but much lower than the second critical speed.

According to the above assumptions, only the first shaft mode is involved and the second mode will not be excited. When a disc is installed in the middle of a shaft, the gyroscopic effect of disc does not exist or is very weak. With this in mind, the gyroscopic effect of the disc is ignored in the process of dynamic modeling of rotor-casing system.

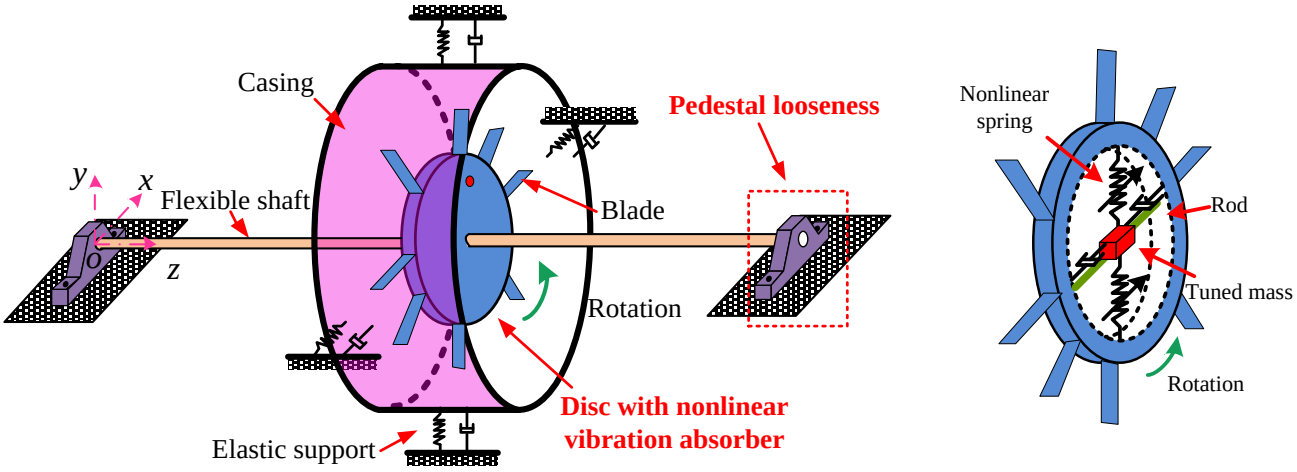

(a) Rotor-casing model (b) Disc with nonlinear vibration absorber

Fig. 1. Schematic diagram of a rotor-casing system in the presence of nonlinear vibration absorber: (a) rotor-casing model, and (b) disc with nonlinear vibration absorber.

2.1 Blade-casing rub model

First of all, the mathematical model for describing the blade-casing rub in the presence of non-uniform gap is given in this part. For the purpose of gas path sealing, oxidation and corrosion control, the coating technology has been gradually recognized and widely adopted in the modern aviation industry [48]. However, due to coating inhomogeneity, aerodynamic load and thermal load, an initial gap between blades and casing may appear and its spatial distribution is non-uniform rather than ideally uniform in the circumstantial direction. Then several straight blades may collide with the casing, as shown in Fig. 2(a).

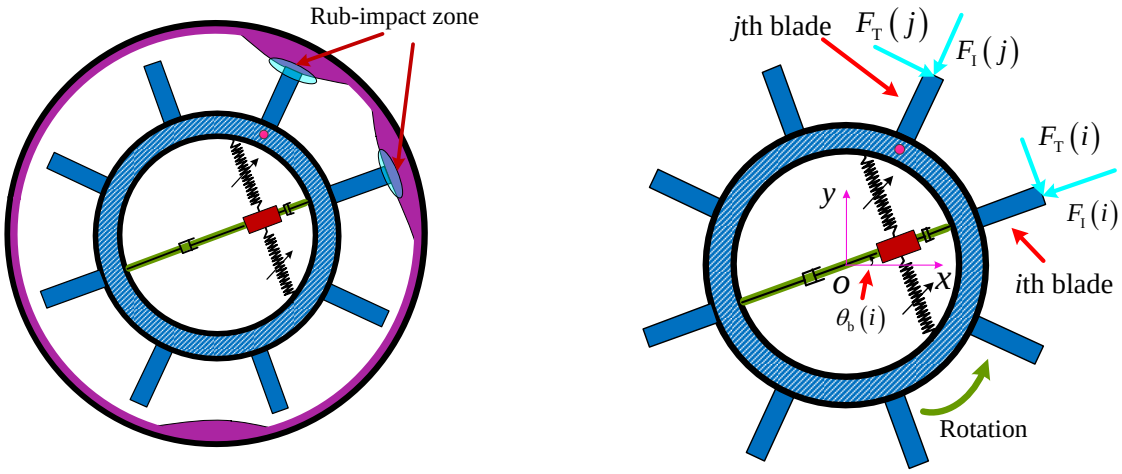

(a) blade-casing rub diagram (b) force analysis diagram

Fig. 2. Schematic diagram of rub-impact between rotating blades and casing in the presence of non-uniform initial gap: (a) blade-casing rub diagram, and (b) force analysis diagram.

Assume that the *i*th blade and the *j*th blade collide with the casing simultaneously, as shown in Fig. 2(b). And then a variable $\theta_{\mathrm{b}}(i)$ is defined to describe the position angle of the *i*th blade with respect to the space-fixed axis $o-x$, namely

$$\theta_{\mathrm{b}}(i)=\frac{2\pi}{N}(i-1)+\omega t, \tag{1}$$

where N denotes the number of blades; ω denotes the rotational speed of the rotor.

Fig. 3 illustrates the non-uniform gap between the *i*th blade and the casing. It is clear that there are three segments for describing the gap non-uniformity. Accordingly, the expressions of the non-uniform gap are [49, 50]

$$\delta\left(\theta_{\mathrm{b}}(i)\right)=\begin{cases}\delta_0-\delta_{\max}, & \left|\theta_{\mathrm{b}}(i)-\phi\right|<\dfrac{\gamma}{2} \quad (\text{Segment 1})\\ \delta_0-\delta_{\max}\left[0.5-0.5\cos\dfrac{2\pi\left(\theta_{\mathrm{b}}(i)-\phi\right)}{\gamma}\right], & \dfrac{\gamma}{2}<\left|\theta_{\mathrm{b}}(i)-\phi\right|<\gamma \quad (\text{Segment 2})\\ \delta_0. & \left|\theta_{\mathrm{b}}(i)-\phi\right|>\gamma \quad (\text{Segment 3})\end{cases} \tag{2}$$

When the gap non-uniformity is not taken into consideration, the initial gap between blades and casing is set to δ_0. On this basis, the gap non-uniformity is considered and the maximum magnitude of the non-uniform gap is expressed as $\delta_{\max}$. Meanwhile, the location and the range of the non-uniform gap are defined as ϕ and γ, respectively.

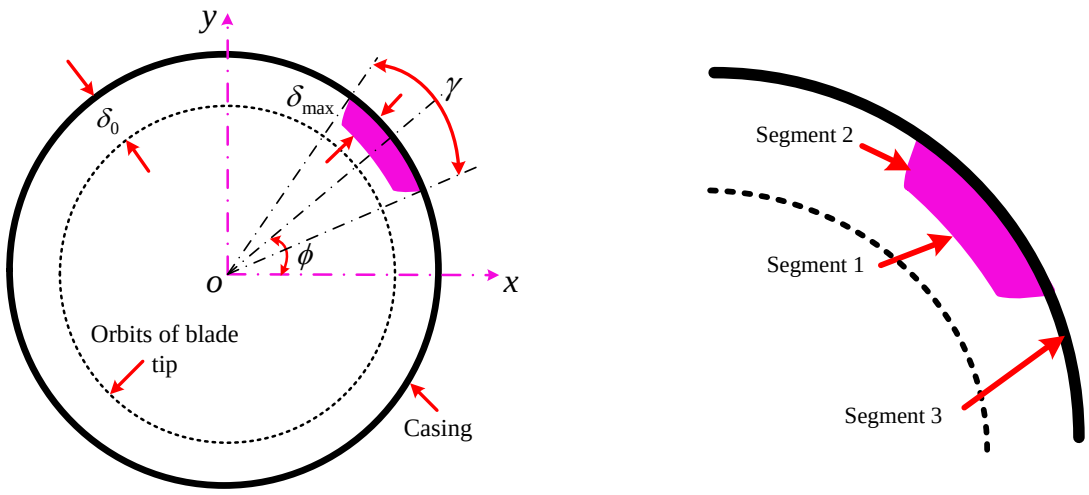

(a) illustration of variables describing the non-uniform gap

(b) three segments in the non-uniform gap

Fig. 3. Schematic diagram of the non-uniform gap: (a) illustration of variables describing the non-uniform gap, and (b) three segments in the non-uniform gap.

If the radial displacement of the *i*th blade $\delta_{\mathrm{b}}(i)$ is larger than the non-uniform gap $\delta\left(\theta_{\mathrm{b}}(i)\right)$ at this moment, blade-casing rub happens and then the corresponding force is given by

$$\begin{cases} F_{\mathrm{I}}(i) = k_{\mathrm{I}}(i)\left(\delta_{\mathrm{b}}(i) - \delta\left(\theta_{\mathrm{b}}(i)\right)\right), \\ F_{\mathrm{T}}(i) = \mu \operatorname{sgn}(v_{\mathrm{rel}}) k_{\mathrm{I}}(i)\left(\delta_{\mathrm{b}}(i) - \delta\left(\theta_{\mathrm{b}}(i)\right)\right), \end{cases} \tag{3}$$

where $k_{\mathrm{I}}(i)$ denotes the impact stiffness of the *i*th blade; μ denotes the kinetic coefficient of friction; sgn denotes the sign function.

Otherwise, there is no contact between the *i*th blade and the casing. Then the above equation can be changed to

$$\begin{cases} F_{\mathrm{I}}(i) = 0, \\ F_{\mathrm{T}}(i) = 0. \end{cases} \tag{4}$$

When calculating the impact displacement given in Eq. (3), the radial displacement of the *i*th blade obeys the following expression:

$$\delta_{\mathrm{b}}(i) = x_{\mathrm{d}} \cos\left(\theta_{\mathrm{b}}(i)\right) + y_{\mathrm{d}} \sin\left(\theta_{\mathrm{b}}(i)\right), \tag{5}$$

where x_{d} and y_{d} denote the lateral and vertical displacements of the disc, respectively.

According to the Coulomb law, the tangential frictional force is mainly determined by the normal impact force and coefficient of friction. Therefore, the tangential relative velocity v_{rel} at the contact point between the *i*th blade and the casing is given by

$$v_{\mathrm{rel}} = \omega\left(R_{\mathrm{d}} + l_{\mathrm{b}}(i)\right) + \dot{y}_{\mathrm{d}} \cos\left(\theta_{\mathrm{b}}(i)\right) - \dot{x}_{\mathrm{d}} \sin\left(\theta_{\mathrm{b}}(i)\right), \tag{6}$$

where R_{d} denotes the outer radius of the disc; $l_{\mathrm{b}}(i)$ denotes the length of the *i*th blade; $\dot{x}_{\mathrm{d}}$ and $\dot{y}_{\mathrm{d}}$ denote the lateral and vertical velocities of the disc, respectively.

For N blades uniformly mounted on the disc, it is necessary to judge whether all these blades will collide with the casing in the whirling motion of the system. As a result, the total rub-impact force in the two directions $o-x$ and $o-y$ can be expressed as

$$F_x = \sum_{i=1}^{N}\left(-F_{\mathrm{I}}(i)\cos\left(\theta_{\mathrm{b}}(i)\right) + F_{\mathrm{T}}(i)\sin\left(\theta_{\mathrm{b}}(i)\right)\right), \tag{7}$$

and

$$F_y = \sum_{i=1}^{N}\left(-F_{\mathrm{I}}(i)\sin\left(\theta_{\mathrm{b}}(i)\right) - F_{\mathrm{T}}(i)\cos\left(\theta_{\mathrm{b}}(i)\right)\right). \tag{8}$$

2.2 Pedestal looseness model

In this part, the mathematical model for describing pedestal looseness is further established. Because of possible poor installation quality or long period of vibration, the looseness fault is more likely to happen at the pedestal, as shown in Fig. 4. The looseness fault could immediately weaken the elastic constraint stiffness of pedestal and promote the violent vibration to a great extent.

According to the inherent property of the looseness fault, the constraint stiffness of the pedestal having looseness fault can be expressed as [51]

$$k_{\mathrm{p}}=\begin{cases}k_{\mathrm{p2}} & y_{\mathrm{p}}>\delta_{\mathrm{L}},\\ k_{\mathrm{p1}} & 0\le y_{\mathrm{p}}\le\delta_{\mathrm{L}},\\ k_{\mathrm{p2}} & y_{\mathrm{p}}<0,\end{cases}\tag{9}$$

where y_{p} denotes the vertical displacement of the loose pedestal; δ_{L} denotes the initial loose gap; k_{p1} denotes the constraint stiffness under the loose state; k_{p2} denotes the constraint stiffness under the locked state.

(a) no looseness fault (b) looseness fault

Fig. 4. Schematic diagram of pedestal model supporting the rotor system: (a) no looseness fault, and (b) looseness fault.

Similarly, the expression of the constraint damping of the pedestal considering looseness fault is given by

$$c_{\mathrm{p}}=\begin{cases}c_{\mathrm{p2}} & y_{\mathrm{p}}>\delta_{\mathrm{L}},\\ c_{\mathrm{p1}} & 0\le y_{\mathrm{p}}\le\delta_{\mathrm{L}},\\ c_{\mathrm{p2}} & y_{\mathrm{p}}<0,\end{cases}\tag{10}$$

where c_{p1} denotes the constraint damping under the loose state; c_{p2} denotes the constraint damping under the locked state.

2.3 Rotor-casing model in the presence of nonlinear vibration absorber

For reducing the large vibration amplitude caused by the above coupled fault, the nonlinear vibration absorber is introduced to the rotor-casing system. As shown in Fig. 1(b), a rod is installed in the disc and rigidly connected with the rotor shaft. This rod passes through the centre of the absorber. In addition, two nonlinear springs and two viscous dampers are adopted between the absorber and the disc. Under the centrifugal force given by the disc eccentricity, the whirling motion of the rotor system happens. In this condition, the nonlinear vibration absorber can only slide along the fixed rod.

Fig 5 shows two kinds of system states, including motion before whirling and in whirling. At the initial moment, the rod is assumed to be parallel to the coordinate axis of $o-x$. Meanwhile, there is an initial offset between the centre of absorber and the centre of disc. It can be defined as r_0, as shown in Fig. 5(a).

In order to describe the whirling motion of the system (see Fig. 5(b)), the position vectors of the disc, absorber mass, imbalance mass, and casing can be expressed as

$$\begin{cases} \mathbf{oo}_1 = \left(x_\mathrm{d}, y_\mathrm{d}\right), \\ \mathbf{o}_1\mathbf{o}_2 = \left(\left(r_0 + \delta_\mathrm{N}\right)\cos\omega t, \left(r_0 + \delta_\mathrm{N}\right)\sin\omega t\right), \\ \mathbf{o}_1\mathbf{o}_3 = \left(e\cos\left(\omega t + \beta\right), e\sin\left(\omega t + \beta\right)\right), \\ \mathbf{oo}_4 = \left(x_\mathrm{c}, y_\mathrm{c}\right), \end{cases} \tag{11}$$

where x_d and y_d denote the lateral and vertical displacements of the disc; x_c and y_c denotes the lateral and vertical displacements of the casing; δ_N denotes the relative displacement between the absorber centre and the disc centre; e denotes the disc eccentricity; β denotes the relative angle between the radial directions of the absorber mass and the imbalance mass.

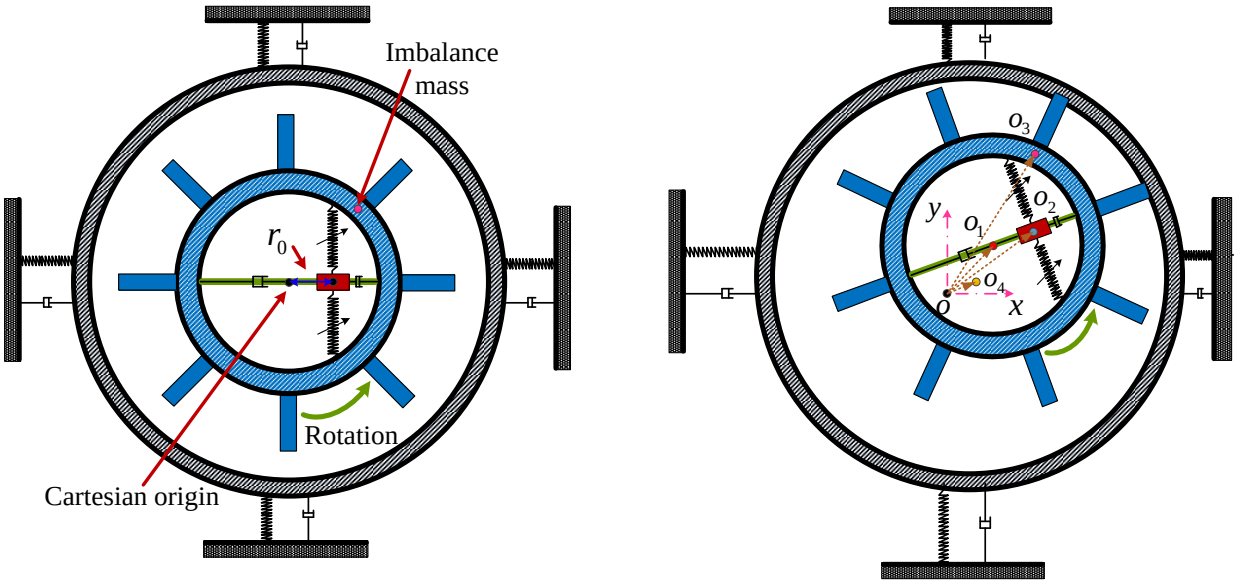

(a) before whirling motion (b) in whirling motion

Fig. 5. Schematic diagram of motion states of the rotor-casing system with nonlinear vibration absorber: (a) before whirling motion and (b) in whirling motion.

After that, the equations of motion of rotor-casing system in the presence of the nonlinear vibration absorber are derived by utilizing the Lagrange's equation. The system shown in Fig. 1 can be divided into five subsystems, including disc, casing, imbalance mass, nonlinear vibration absorber, and loose pedestal. From this viewpoint, the total kinetic energy of the system can be expressed as

$$T = T_\mathrm{d} + T_\mathrm{i} + T_\mathrm{N} + T_\mathrm{c} + T_\mathrm{p}, \tag{12}$$

where the kinetic energies of the disc and the imbalance mass are given by

$$T_\mathrm{d} = \frac{1}{2}m_\mathrm{d}\dot{x}_\mathrm{d}^2 + \frac{1}{2}m_\mathrm{d}\dot{y}_\mathrm{d}^2 + \frac{1}{2}J_\mathrm{d}\omega^2, \tag{13}$$

$$T_\mathrm{i} = \frac{1}{2}m_\mathrm{e}\left(\dot{x}_\mathrm{d} - e\omega\sin\left(\omega t + \beta\right)\right)^2 + \frac{1}{2}m_\mathrm{e}\left(\dot{y}_\mathrm{d} + e\omega\cos\left(\omega t + \beta\right)\right)^2. \tag{14}$$

For the nonlinear vibration absorber installed in the disc, according to the position vector (i.e., Eq. (11)), the kinetic energy can be expressed as

$$T_{\mathrm{N}}=\frac{1}{2}m_{\mathrm{N}}\left(\dot{x}_{\mathrm{d}}+\dot{\delta}_{\mathrm{N}}\cos\omega t-\left(\delta_{\mathrm{N}}+r_0\right)\omega\sin\omega t\right)^2+\frac{1}{2}m_{\mathrm{N}}\left(\dot{y}_{\mathrm{d}}+\dot{\delta}_{\mathrm{N}}\sin\omega t+\left(\delta_{\mathrm{N}}+r_0\right)\omega\cos\omega t\right)^2. \quad (15)$$

In addition, the kinetic energies of the casing and the loose pedestal are derived as

$$T_{\mathrm{c}}=\frac{1}{2}m_{\mathrm{c}}\dot{x}_{\mathrm{c}}^2+\frac{1}{2}m_{\mathrm{c}}\dot{y}_{\mathrm{c}}^2, \quad (16)$$

$$T_{\mathrm{P}}=\frac{1}{2}m_{\mathrm{p}}\dot{y}_{\mathrm{p}}^2, \quad (17)$$

where m_{d} denotes the mass of the disc; m_{e} denotes the imbalance mass; m_{N} denotes the mass of the absorber; m_{c} denotes the mass of the casing; m_{p} denotes the mass of the loose pedestal; $\dot{\delta}_{\mathrm{N}}$ denotes the relative velocity of the absorber centre and the disc centre; $\dot{x}_{\mathrm{c}}$ and $\dot{y}_{\mathrm{c}}$ denotes the lateral and vertical velocities of the casing; $\dot{y}_{\mathrm{p}}$ denotes the vertical velocity of the pedestal.

Combined with the above five parts, the potential energy of the system is further derived. The restoring force of the nonlinear springs used in the nonlinear vibration absorber can be given as

$$F_{\mathrm{N}}=k_{\mathrm{N}}\delta_{\mathrm{N}}^3, \quad (18)$$

where k_{N} denotes the nonlinear stiffness of the nonlinear vibration absorber.

In this condition, the potential energy of the nonlinear vibration absorber is given by

$$V_{\mathrm{N}}=\int_0^{\delta_{\mathrm{N}}}F_{\mathrm{N}}d\delta_{\mathrm{N}}=\frac{k_{\mathrm{N}}\delta_{\mathrm{N}}^4}{4}. \quad (19)$$

Due to the severe imbalance excitation and the pedestal looseness, the whirling motion with large amplitude is more likely to occur in the flexible shaft. At this point, the geometrical relation between the displacement of the shaft and its strain becomes nonlinear rather than linear. According to the authors' previous work [52], the equation of motion of the massless flexible shaft having geometric nonlinearity is

$$\left(EIw''-2EI\left(w'\right)^2w''\right)''+\left(2EI\left(w''\right)^2w'-\frac{1}{2}EA\left(w'\right)^3\right)'=Q_{\mathrm{nc}}, \quad (20)$$

where EI denotes the bending stiffness of the shaft; w denotes the elastic deflection of the shaft; A denotes the area of the cross section; Q_{nc} denotes the non-conservative force.

On this basis, Eq. (20) is further converted into the ordinary differential equation by using the first mode of a simply-supported beam. Thus, the restoring force of the shaft obeys the following form:

$$F_{\mathrm{s}}=k_{\mathrm{L}}\delta_{\mathrm{d}}+k_{\alpha}\delta_{\mathrm{d}}^3+c\dot{\delta}_{\mathrm{d}}, \quad (21)$$

where k_{L} and k_{α} are seen as the structural linear stiffness and the geometrical nonlinear stiffness. They can be expressed as

$$\begin{cases} k_{\mathrm{L}} = \dfrac{EI\pi^4}{2l^3}, \\ k_{\alpha} = \dfrac{3EA\pi^4}{16l^3} - \dfrac{EI\pi^6}{2l^5}, \end{cases} \tag{22}$$

Obviously, the structural linear stiffness k_{L} is consistent with that in mechanics of material. In addition, the geometrical nonlinear stiffness k_{α} is determined by the length of shaft l, area of cross section A, and diametrical moment of inertia I.

According to Eqs. (19) and (21), the total potential energy of the system, including the shaft, nonlinear vibration absorber, casing and loose pedestal, can be expressed as

$$V = \frac{1}{2}k_{\mathrm{L}}\left(x_{\mathrm{d}}^2 + \left(y_{\mathrm{d}} - y_{\mathrm{p}}\right)^2\right) + \frac{1}{4}k_{\alpha}\left(x_{\mathrm{d}}^2 + \left(y_{\mathrm{d}} - y_{\mathrm{p}}\right)^2\right)^2 + \frac{1}{4}k_{\mathrm{N}}\delta_{\mathrm{N}}^4 + \frac{1}{2}k_{\mathrm{c}}\left(x_{\mathrm{c}}^2 + y_{\mathrm{c}}^2\right) + \frac{1}{2}k_{\mathrm{p}}y_{\mathrm{p}}^2, \tag{23}$$

where k_{c} denotes the support stiffness of the casing; k_{p} denotes the constraint stiffness of the pedestal.

Moreover, due to the existence of the viscous damping, the total dissipative energy of the system is given by

$$D = \frac{1}{2}c\dot{x}_{\mathrm{d}}^2 + \frac{1}{2}c\left(\dot{y}_{\mathrm{d}} - \dot{y}_{\mathrm{p}}\right)^2 + \frac{1}{2}c_{\mathrm{N}}\dot{\delta}_{\mathrm{N}}^2 + \frac{1}{2}c_{\mathrm{c}}\dot{x}_{\mathrm{c}}^2 + \frac{1}{2}c_{\mathrm{c}}\dot{y}_{\mathrm{c}}^2 + \frac{1}{2}c_{\mathrm{p}}\dot{y}_{\mathrm{p}}^2, \tag{24}$$

where c_{N} denotes the damping of the nonlinear vibration absorber; c_{c} denotes the damping of the casing.

Then substitute Eqs. (12), (23) and (24) to the Lagrange's equations as follows:

$$\frac{d}{dt}\left(\frac{\partial\left(T-V\right)}{\partial\dot{q}_{\mathrm{i}}}\right) - \frac{\partial\left(T-V\right)}{\partial q_{\mathrm{i}}} + \frac{\partial D}{\partial\dot{q}_{\mathrm{i}}} = Q, \tag{25}$$

where q_{i} denotes the ith generalized coordinate; Q denotes the generalized excitation of the system.

Consequently, the governing equations of motion of the rotor-casing system in the presence of nonlinear vibration absorber can be expressed in the matrix form, namely

$$\mathbf{M}\ddot{\mathbf{u}} + \mathbf{C}\dot{\mathbf{u}} + \mathbf{K}\mathbf{u} = \mathbf{F}_{\mathbf{g}}, \tag{26}$$

where the generalized displacement vector of the system is

$$\mathbf{u}^{\mathrm{T}} = \left[x_{\mathrm{d}}, y_{\mathrm{d}}, \delta_{\mathrm{N}}, x_{\mathrm{c}}, y_{\mathrm{c}}, y_{\mathrm{p}}\right], \tag{27}$$

which suggests that the dynamic model proposed in this paper has six degrees of freedom. Additionally, the mass, damping and stiffness matrices of the system are respectively written as

$$\mathbf{M} = \begin{bmatrix} m_{\mathrm{d}} + m_{\mathrm{e}} + m_{\mathrm{N}} & 0 & m_{\mathrm{N}}\cos\omega t & 0 & 0 & 0 \\ 0 & m_{\mathrm{d}} + m_{\mathrm{e}} + m_{\mathrm{N}} & m_{\mathrm{N}}\sin\omega\mathrm{t} & 0 & 0 & 0 \\ m_{\mathrm{N}}\cos\omega t & m_{\mathrm{N}}\sin\omega t & m_{\mathrm{N}} & 0 & 0 & 0 \\ 0 & 0 & 0 & m_{\mathrm{c}} & 0 & 0 \\ 0 & 0 & 0 & 0 & m_{\mathrm{c}} & 0 \\ 0 & 0 & 0 & 0 & 0 & m_{\mathrm{p}} \end{bmatrix}, \tag{28}$$

$$\mathbf{C}=\begin{bmatrix} c & 0 & -2m_{\mathrm{N}}\omega\sin\omega t & 0 & 0 & 0 \\ 0 & c & 2m_{\mathrm{N}}\omega\cos\omega t & 0 & 0 & -c \\ 0 & 0 & c_{\mathrm{N}} & 0 & 0 & 0 \\ 0 & 0 & 0 & c_{\mathrm{c}} & 0 & 0 \\ 0 & 0 & 0 & 0 & c_{\mathrm{c}} & 0 \\ 0 & -c & 0 & 0 & 0 & c+c_{\mathrm{p}} \end{bmatrix}, \tag{29}$$

$$\mathbf{K}=\begin{bmatrix} k_{\mathrm{L}}+k_{\alpha}\left(x_{\mathrm{d}}^2+\left(y_{\mathrm{d}}-y_{\mathrm{p}}\right)^2\right) & 0 & -m_{\mathrm{N}}\omega^2\cos\omega t & 0 & 0 & 0 \\ 0 & k_{\mathrm{L}}+k_{\alpha}\left(x_{\mathrm{d}}^2+\left(y_{\mathrm{d}}-y_{\mathrm{p}}\right)^2\right) & -m_{\mathrm{N}}\omega^2\sin\omega t & 0 & 0 & -k_{\mathrm{L}}-k_{\alpha}\left(x_{\mathrm{d}}^2+\left(y_{\mathrm{d}}-y_{\mathrm{p}}\right)^2\right) \\ 0 & 0 & k_{\mathrm{N}}\delta_{\mathrm{N}}^2-m_{\mathrm{N}}\omega^2 & 0 & 0 & 0 \\ 0 & 0 & 0 & k_{\mathrm{c}} & 0 & 0 \\ 0 & 0 & 0 & 0 & k_{\mathrm{c}} & 0 \\ 0 & -k_{\mathrm{L}}-k_{\alpha}\left(x_{\mathrm{d}}^2+\left(y_{\mathrm{p}}-y_{\mathrm{d}}\right)^2\right) & 0 & 0 & 0 & k_{\mathrm{L}}+k_{\mathrm{p}}+k_{\alpha}\left(x_{\mathrm{d}}^2+\left(y_{\mathrm{p}}-y_{\mathrm{d}}\right)^2\right) \end{bmatrix}. \tag{30}$$

Moreover, the generalized force vector acting on the rotor-casing system with the nonlinear vibration absorber can be expressed as

$$\mathbf{F_g}=\begin{bmatrix} m_{\mathrm{e}}e\omega^2\cos\left(\omega t+\beta\right)+m_{\mathrm{N}}\omega^2 r_0\cos\omega t+F_x \\ m_{\mathrm{e}}e\omega^2\sin\left(\omega t+\beta\right)+m_{\mathrm{N}}\omega^2 r_0\sin\omega t+F_y \\ m_{\mathrm{N}}r_0\omega^2 \\ -F_x \\ -F_y \\ 0 \end{bmatrix}. \tag{31}$$

It is clear that the generalized force vector includes the centrifugal force provided by the disc eccentricity, two components of rub-impact force, and three particular additional excitations. It should be noted that these additional excitations are determined by the initial offset of the nonlinear vibration absorber.

2.4 Rotor-casing model in the absence of nonlinear vibration absorber

To reveal the vibration reduction effect brought about by the nonlinear vibration absorber, a comparison of the vibration responses of the rotor-casing system with and without absorber is conducted. So the dynamic model of the rotor-casing system in the absence of nonlinear vibration absorber is set up in this section.

Through the similar derivation just like in section 2.3, the governing equations of motion of the rotor-casing system without absorber are written as

$$\mathbf{M}^*\ddot{\mathbf{v}}+\mathbf{C}^*\dot{\mathbf{v}}+\mathbf{K}^*\mathbf{v}=\mathbf{F}_{\mathrm{g}}^*. \tag{32}$$

In this case, there will be five degrees of freedom in the system. And then the generalized

displacement vector is changed to

$$\mathbf{v}^{\mathrm{T}} = \left[x_{\mathrm{d}}, y_{\mathrm{d}}, x_{\mathrm{c}}, y_{\mathrm{c}}, y_{\mathrm{p}} \right]. \tag{33}$$

At the same time, the mass, damping and stiffness matrices of the rotor-casing system in the absence of the absorber take the following forms:

$$\mathbf{M}^{*} = \begin{bmatrix} m_{\mathrm{d}}+m_{\mathrm{e}} & 0 & 0 & 0 & 0 \\ 0 & m_{\mathrm{d}}+m_{\mathrm{e}} & 0 & 0 & 0 \\ 0 & 0 & m_{\mathrm{c}} & 0 & 0 \\ 0 & 0 & 0 & m_{\mathrm{c}} & 0 \\ 0 & 0 & 0 & 0 & m_{\mathrm{p}} \end{bmatrix}, \tag{34}$$

$$\mathbf{C}^{*} = \begin{bmatrix} c & 0 & 0 & 0 & 0 \\ 0 & c & 0 & 0 & -c \\ 0 & 0 & c_{\mathrm{c}} & 0 & 0 \\ 0 & 0 & 0 & c_{\mathrm{c}} & 0 \\ 0 & -c & 0 & 0 & c+c_{\mathrm{p}} \end{bmatrix}, \tag{35}$$

$$\mathbf{K}^{*} = \begin{bmatrix} k_{\mathrm{L}} + k_{\alpha}\left(x_{\mathrm{d}}^{2}+\left(y_{\mathrm{d}}-y_{\mathrm{p}}\right)^{2}\right) & 0 & 0 & 0 & 0 \\ 0 & k_{\mathrm{L}} + k_{\alpha}\left(x_{\mathrm{d}}^{2}+\left(y_{\mathrm{d}}-y_{\mathrm{p}}\right)^{2}\right) & 0 & 0 & -k_{\mathrm{L}} - k_{\alpha}\left(x_{\mathrm{d}}^{2}+\left(y_{\mathrm{d}}-y_{\mathrm{p}}\right)^{2}\right) \\ 0 & 0 & k_{\mathrm{c}} & 0 & 0 \\ 0 & 0 & 0 & k_{\mathrm{c}} & 0 \\ 0 & -k_{\mathrm{L}} - k_{\alpha}\left(x_{\mathrm{d}}^{2}+\left(y_{\mathrm{d}}-y_{\mathrm{p}}\right)^{2}\right) & 0 & 0 & k_{\mathrm{L}}+k_{\mathrm{p}} + k_{\alpha}\left(x_{\mathrm{d}}^{2}+\left(y_{\mathrm{p}}-y_{\mathrm{d}}\right)^{2}\right) \end{bmatrix}. \tag{36}$$

When the nonlinear vibration absorber is not considered in the system, the particular additional excitations given in Eq. (31) will disappear. Then the expression of the new generalized force vector is

$$\mathbf{F}_{\mathbf{g}}^{*} = \begin{bmatrix} m_{\mathrm{e}}e\omega^{2}\cos\left(\omega t+\beta\right)+F_{x} \\ m_{\mathrm{e}}e\omega^{2}\sin\left(\omega t+\beta\right)+F_{y} \\ -F_{x} \\ -F_{y} \\ 0 \end{bmatrix}. \tag{37}$$

From Eqs. (32)-(37), it can be seen that the dynamic model of the system without the nonlinear vibration absorber is very similar to that given in [53], in which the accuracy of the theoretical model has been verified by the vibration experiment performed on a rotor test rig. In other words, the dynamic model proposed in this paper is valid and could be used in the following numerical simulation.

3. Vibration characteristic without nonlinear vibration absorber

Due to several strong nonlinear factors (i.e., pedestal looseness and blade-casing rub), it is impossible to determine the dynamic characteristics of the rotor system using an analytical method. Therefore, the Runge-Kutta method is used in the dynamics simulation, in which the linear interpolation method is utilized to estimate the occurrence of rub-impact fault. Meanwhile, the time integration step is set to $2\pi/(1000\omega)$. The main structural parameters used in this paper are given in the Appendix.

In order to fully understand the vibration characteristics of the rotor-casing system without nonlinear vibration absorber, a sweep frequency analysis is conducted in advance, where the frequency range is $\omega=[100,\ 300]$ rad/s. The influences of the geometrical nonlinearity of the shaft and the pedestal looseness on the amplitude-frequency curves are shown in Fig. 6, in which the horizontal axis represents the rotational speed and the vertical axis represents the vertical displacement of disc.

When the nonlinear factors involved in the system are put on the back burner, the resonant frequency of the system is $\omega=149$ rad/s. According to the linear vibration theory, it is mainly determined by the structural linear stiffness k_{L}, disc mass m_{d} and imbalance mass m_{e}. On this basis, the influence of geometrical nonlinearity is further analysed. Due to the additional geometrical nonlinear stiffness k_{α}, the resonant frequency increases from 149 rad/s to 160 rad/s, as shown in Fig. 6(a). Therefore, it may be not accurate to predict the critical speed only by the linear stiffness and the mass of the system when the serious whirling motion occurs.

Next the comparison of the amplitude-frequency curve of the system without and with pedestal looseness is accomplished. The looseness fault could immediately weaken the constraint stiffness of the pedestal, which further leads to increase of vibration amplitude. Fig. 6(b) shows the change of amplitude-frequency curve of the rotor system with or without pedestal looseness. The resonant frequency decrease from $\omega=160$ rad/s to $\omega=152$ rad/s. Meanwhile, the resonant amplitude of disc increases from 4.53 mm to 5.87 mm.

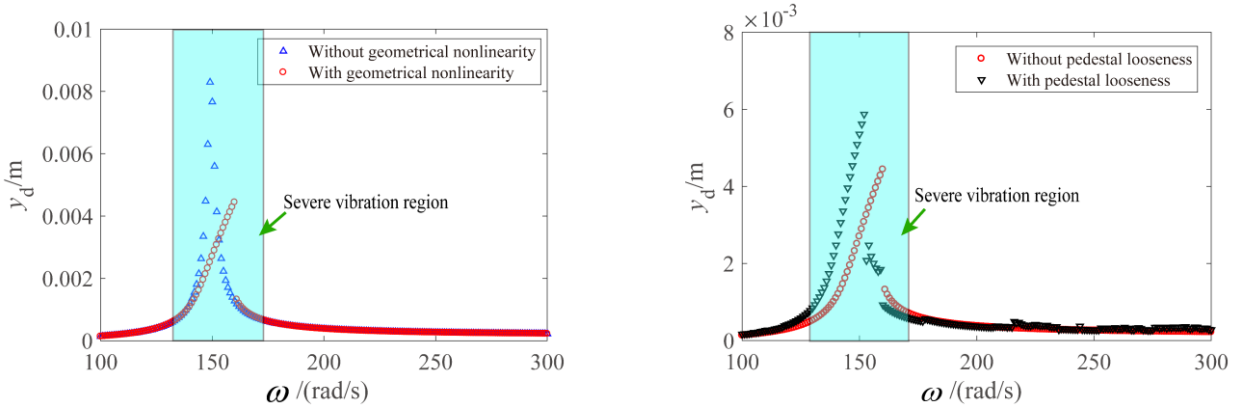

(a) without and with geometrical nonlinearity (b) without and with pedestal looseness

Fig. 6. Amplitude-frequency curve of the system: (a) without and with geometrical nonlinearity, and (b) without and with pedestal looseness.

For the above response peaks of four conditions, the time histories of vertical displacement of disc are introduced for analyzing the vibration characteristics of the system. As shown Fig. 7, the regular 1*T*-periodic motion is observed in the vibration response of the system. However, due to pedestal looseness, the increase of vibration amplitude by $22.8\,\%$ is extremely unfavorable for the safe operation of rotating machinery.

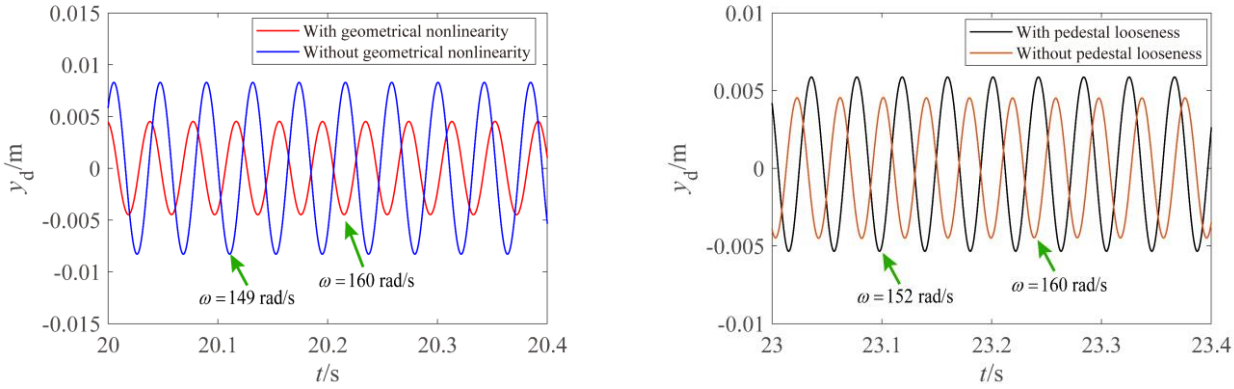

(a) with and without geometrical nonlinearity (b) with and without pedestal looseness

Fig. 7. Time histories of vertical displacement of disc: (a) with and without geometrical nonlinearity, and (b) with and without pedestal looseness.

The pedestal looseness not only aggravates the whirling motion of the rotor system, but also makes the blade-casing rub happen more easily. Therefore, it is of significance to further investigate the vibration response of the system subjected to pedestal looseness and blade-casing rub. When the rub-impact fault happens, the rotor system and the casing are coupled, which may lead to more complicated motion to some extent.

When the rotational speed is $\omega=152$ rad/s, the dynamic responses of the rotor-casing system having coupled fault are shown in Fig. 8. Since that the imbalance force is much larger than the rub-impact force, the rotor system remains regular 1*T*-periodic motion, as shown in Fig. 8(a). From the whirling orbit of the system, it can be seen that rub-impact fault only occurs at the position of non-uniform initial gap. The fault form is recognized as partial one. As a result, the pulse-like motion of casing and pulse-like impact force can be observed in Fig. 8(c) and (d). Since the rotor system and the casing are closely coupled, the pedestal looseness will not only aggravate the disc vibration, but also enhance the casing vibration. Meanwhile, the resultant impact force increases and becomes more intensive. The main reason is that the pedestal looseness causes the blades to collide with the casing in several places, such as the first zone and the second zone.

Keeping the other parameters used in Table 1 unchanged, the rotational speed of the rotor system is reset to $\omega=143$ rad/s, which means that the working state of the system is far away from the resonance region. Accordingly, the dynamic characteristics of the system are shown in Fig. 9. For the case of no pedestal looseness, the whirling amplitude of the disc is smaller than the initial gap. Therefore, the blade-casing rub will not happen at this speed. The rotor and the casing are not coupled together, so the casing is in a stationary state. In the presence of the looseness fault, the whirling amplitude of the disc is synchronously intensified. For this reason, the blades and the casing have a slight collision in the non-uniform gap, that is, the first rub zone. Then the pulse-like motion

of casing and the pulse-like impact force with small amplitude are also found in Fig. 9(c) and (d). The above dynamic phenomena suggest that the existence of the pedestal looseness will not only aggravate the rub-impact degree, but also cause it to occur at a lower speed.

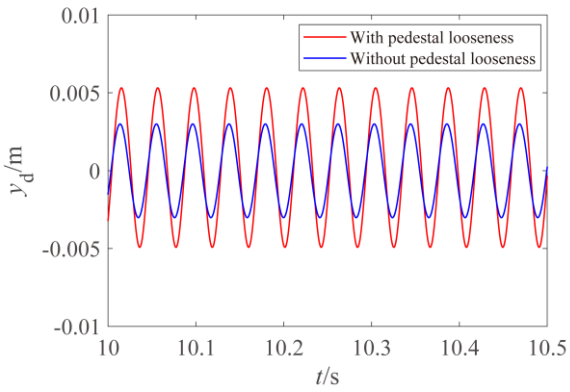

(a) time histories of vertical displacement of disc

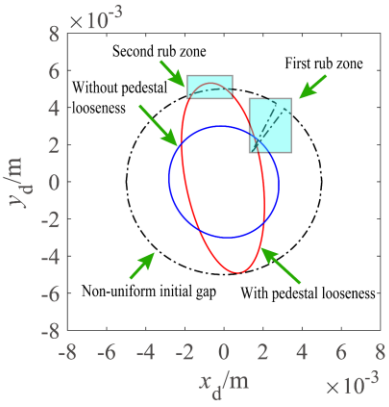

(b) whirling orbit of disc

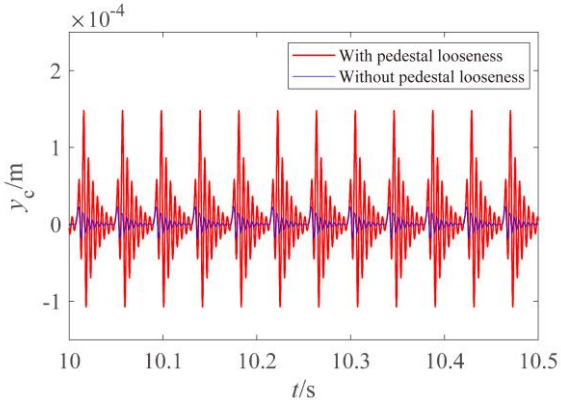

(c) time histories of vertical displacement of casing

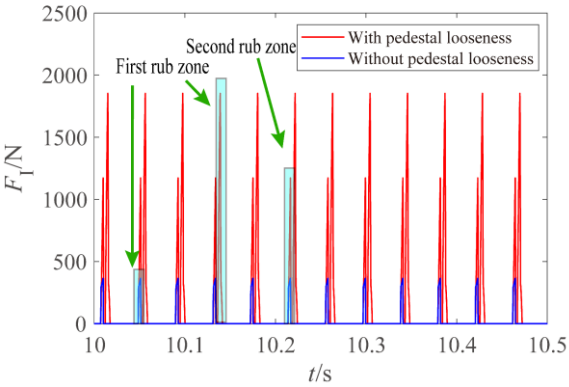

(d) resultant impact force of disc

Fig. 8. Dynamic response of the rotor-casing with imbalance-looseness-rub coupled fault at $\omega = 152$ rad/s: (a) time histories of vertical displacement of disc, (b) whirling orbit of disc, (c) time histories of vertical displacement of casing, and (d) resultant impact force of disc.

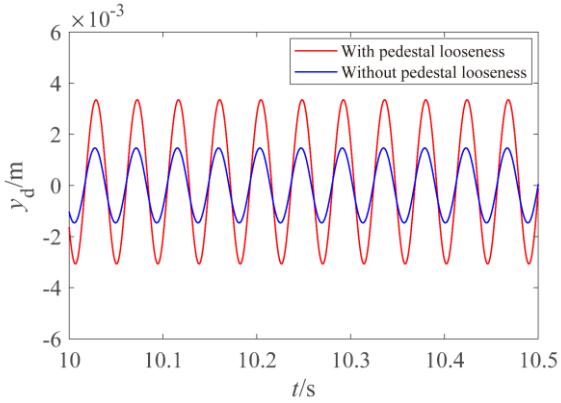

(a) time histories of vertical displacement of disc

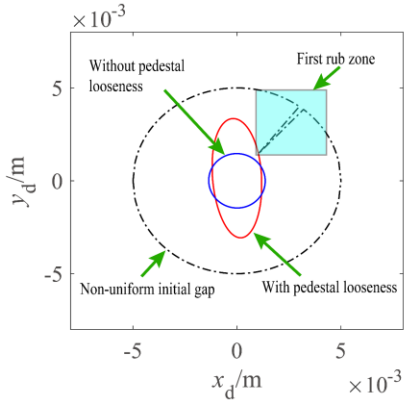

(b) whirling orbit of disc

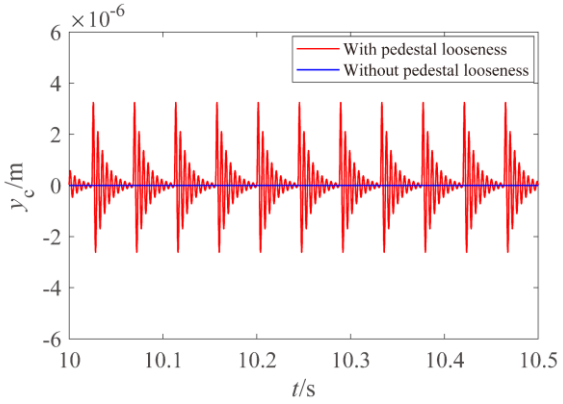

(c) time histories of vertical displacement of casing

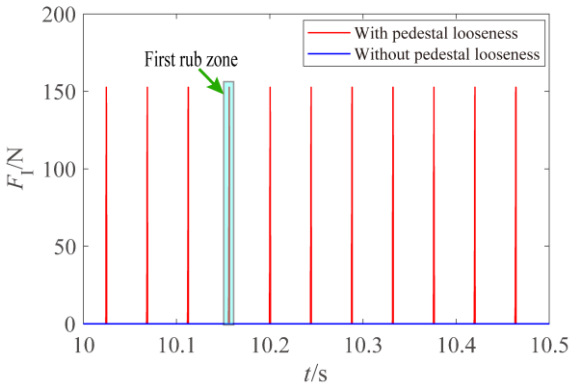

(d) resultant impact force of disc

Fig. 9. Dynamic response of the rotor-casing system with imbalance-looseness-rub coupled fault at $\omega = 143$ rad/s: (a) time histories of vertical displacement of disc, (b) whirling orbit of disc, (c) time histories of vertical displacement of casing, and (d) resultant impact force of disc.

To sum up, blade-casing and pedestal looseness have a potential threat to the safe operation of rotating machinery. The effective vibration suppression of the system, especially in the resonance region, is one of the important measures for realizing the smooth operation of the faulty system. This is of great significance in the actual aviation industry.

4. Vibration mitigation of the rotor system

Next this section focuses on the vibration reduction of the faulty system by means of the nonlinear vibration absorber, in which the displacement of disc and loose pedestal, and the impact force of blades are emphasized. In this way, it is expected to alleviate the damage of coupled fault and improve the stability of the system.

4.1 Parameter optimization of nonlinear vibration absorber

In order to reduce the resonant amplitude at the critical speed, the parameters of the nonlinear vibration absorber are firstly optimized. For convenient analysis, two coefficients η_{k} and η_{m} are adopted to describe the changes of the stiffness and the mass of the absorber, namely

$$\begin{cases} k_{\mathrm{N}} = 0.05\eta_{\mathrm{k}} k_{\mathrm{L}}, \\ m_{\mathrm{N}} = 0.0005\eta_{\mathrm{m}} m_{\mathrm{d}}. \end{cases} \tag{38}$$

According to some publications [33, 54, 55], the ranges of these two coefficients are set to $\eta_{\mathrm{k}} = [1{:}1{:}20]$ and $\eta_{\mathrm{m}} = [1{:}1{:}20]$, respectively. Then the governing equations of motion of the rotor system (i.e., Eq. (26)) are numerically solved under different coefficients η_{k} and η_{m}.

Then the control parameters are optimized in the four cases of installation angle, including $\beta = 0$ rad, $\beta = \pi/8$ rad, $\beta = 3\pi/4$ rad, and $\beta = \pi$ rad. During the optimization process, the absorber mass varies from $0.0005m_{\mathrm{d}}$ to $0.01m_{\mathrm{d}}$ with an increase step size of $0.0005m_{\mathrm{d}}$. The nonlinear stiffness of the absorber varies from $0.05k_{\mathrm{L}}$ to k_{L} with an increase step size of $0.05k_{\mathrm{L}}$. For each pair of absorber mass and absorber stiffness, the maximum vertical vibration

amplitude of the disc at the resonant speed is obtained, as shown in Fig. 10, in which the different colours indicate the different amplitudes. In order to compare the response differences caused by the nonlinear vibration absorber, the grey plane is added in Fig. 10 for representing the maximum vertical vibration amplitude of the disc without the absorber. It is clear that the nonlinear vibration absorber sometimes suppress the system vibration but sometimes not. The main reason is that when the control parameters are not appropriate, the absorber may play a detrimental role like the disc eccentricity, which further intensifies the whirling response of the system. On the contrary, by selecting appropriate parameters, the absorber could make the vibration energy transfer from the main system to the subsystem, achieves vibration reduction.

Therefore, according to effective area for optimization, the installation angle of the nonlinear vibration absorber is set to $\beta = \pi$. Meanwhile, the pair of the absorber mass and the absorber stiffness is $\eta_m = 3$ and $\eta_k = 2$. After obtaining the absorber parameters, the vibration control of the system will be performed in the following part.

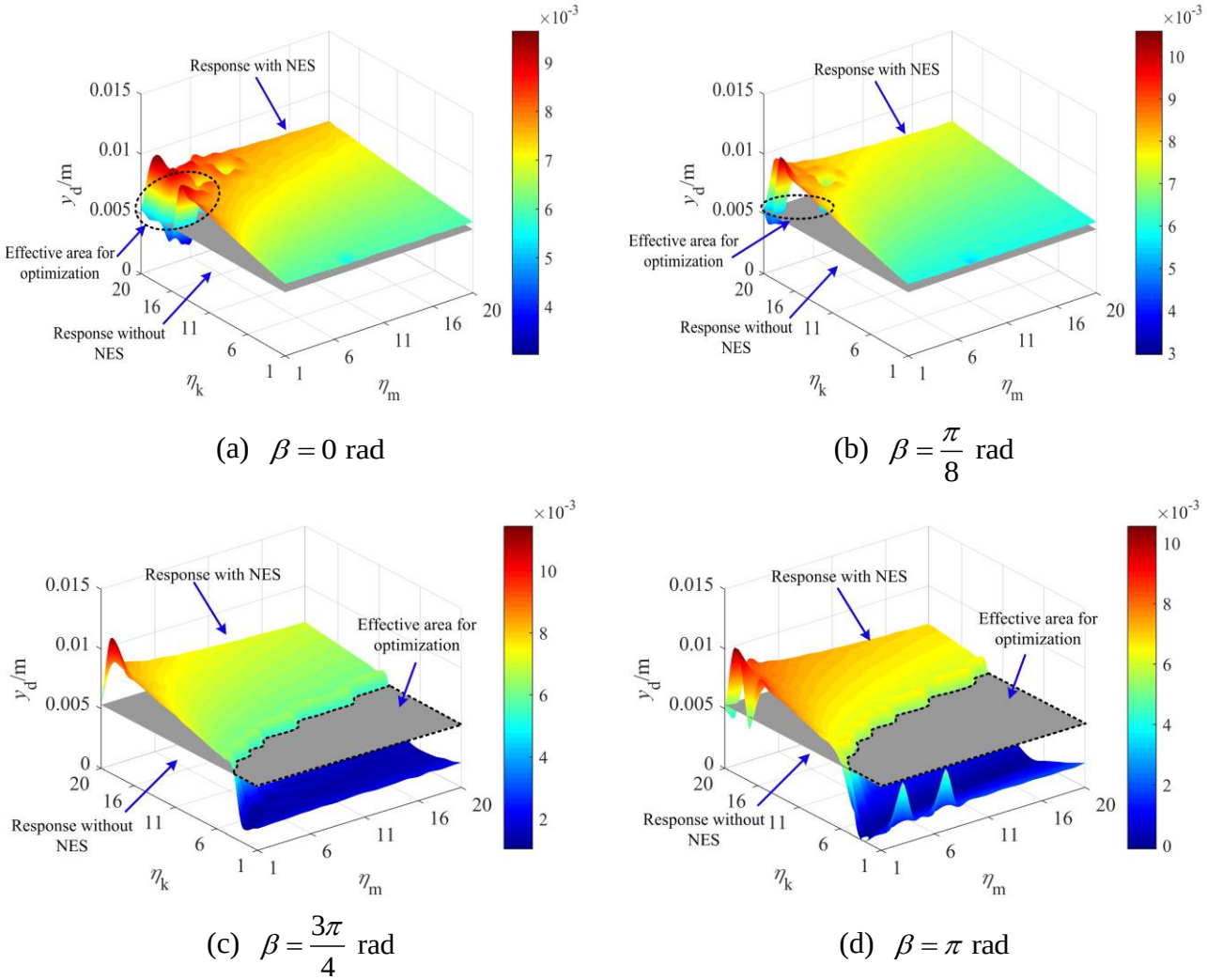

(a) $\beta = 0$ rad (b) $\beta = \frac{\pi}{8}$ rad

(c) $\beta = \frac{3\pi}{4}$ rad (d) $\beta = \pi$ rad

Fig. 10. Optimization results of the rotor system with different installation angle of nonlinear vibration absorber: (a) $\beta = 0$ rad, (b) $\beta = \frac{\pi}{8}$ rad, (c) $\beta = \frac{3\pi}{4}$ rad, and (d) $\beta = \pi$ rad.

4.2 Vibration characteristic of the system with nonlinear vibration absorber

At the beginning, the blade-casing rub in the presence of non-uniform gap is temporarily ignored. Then by employing the nonlinear vibration absorber, the research on vibration mitigation of the rotor-casing system subjected to imbalance-looseness coupled is conducted.

As the rotational speed changes from 100 to 300 rad/s, where the first critical speed is located, the vibration amplitude-frequency responses of the system without and with the nonlinear vibration absorber are depicted in Fig. 11. Due to the existence of the absorber, part of the vibration energy of the main system is transferred. Therefore, the vibration mitigation of the disc in resonant state reaches 49%. Meanwhile, the vibration amplitude of the disc in non-resonant state is effectively reduced as well.

The comparison of vertical vibration responses of the pedestal without and with the absorber is shown in Fig. 11(b). Obviously, the nonlinear vibration absorber can effectively reduce the vibration amplitude of the pedestal. More specifically, the maximum amplitude of the pedestal is limited to at least 45% of that of the pedestal without the absorber. The main reason is that the loose pedestal and the disc are closely coupled by the nonlinear restoring force of the shaft. When the vibration displacement of the disc is affected by the absorber, that of the loose pedestal will also be reduced. The above phenomena reveal the nonlinear vibration absorber could mitigate the damage caused by the looseness fault to some extent.

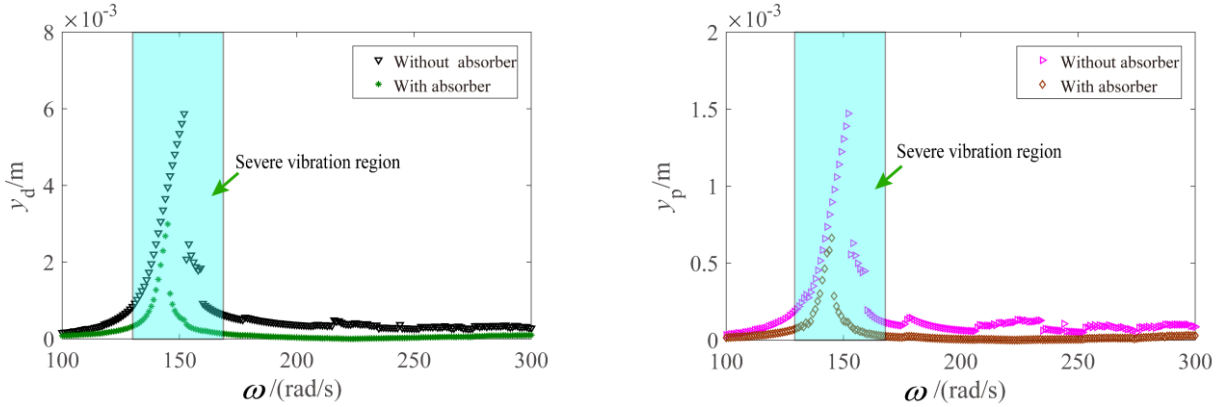

(a) response comparison of disc without and with nonlinear vibration absorber

(b) response comparison of pedestal without and with nonlinear vibration absorber

Fig. 11. Vibration amplitude-frequency responses of the system: (a) response comparison of disc without and with nonlinear vibration absorber, and (b) response comparison of pedestal without and with nonlinear vibration absorber.

To further understand the vibration behavior of disc and loose pedestal, the time histories of vertical displacement of them without and with nonlinear vibration absorber are shown in Fig. 12. It is clear that the disc at resonant state remains the 1*T*-periodic motion, but the vibration amplitude is indeed reduced by the absorber. Since the looseness fault leads to the piecewise form of constraint stiffness, the vibration response of the pedestal appears more complicated. Similarly, the motion pattern of the pedestal is not obviously affected by the absorber, but the vibration amplitude is reduced as well.

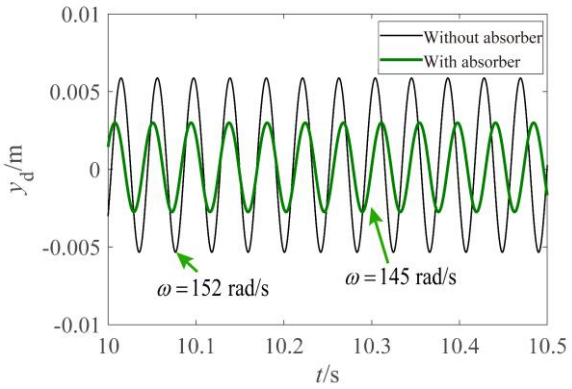

(a) disc without and with nonlinear vibration absorber

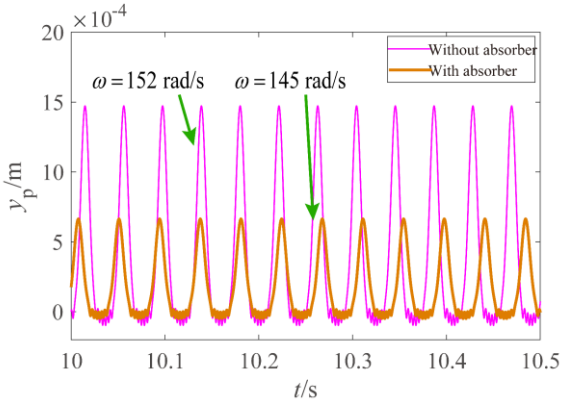

(b) loose pedestal without and with nonlinear vibration absorber

Fig. 12. Time histories of vertical displacement of the system in resonance state: (a) disc without and with nonlinear vibration absorber, and (b) pedestal without and with nonlinear vibration absorber.

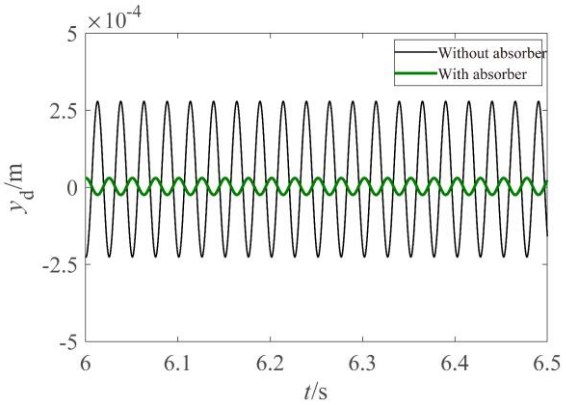

(a) disc without and with nonlinear vibration absorber

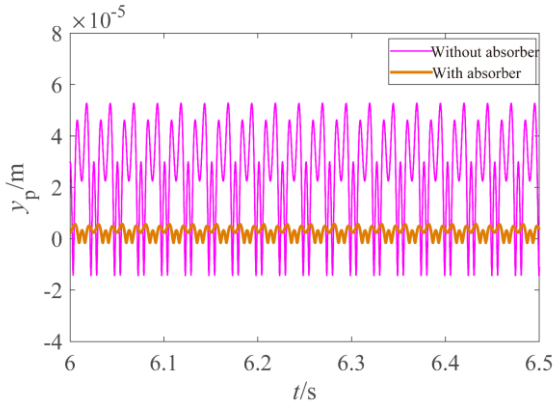

(b) loose pedestal without and with nonlinear vibration absorber

Fig. 13. Time histories of vertical displacement of the system at $\omega = 250$ rad/s : (a) disc without and with nonlinear vibration absorber, and (b) loose pedestal without and with nonlinear vibration absorber.

Then the rotational speed of the rotor system is adjusted to $\omega = 250$ rad/s , which is far away from the resonant vibration region. And the time histories of vertical displacement of disc and loose pedestal are given in Fig. 13. According to a similar mechanism of targeted energy transfer, the vibration amplitude of the disc decreases from 0.28 mm to 0.03 mm . Also due to the coupled relation between disc and pedestal, the effective reduction of vibration amplitude of pedestal is accomplished. Through the study of the system response in resonant and non-resonant regions, it is further confirmed that the nonlinear vibration absorber could effectively work in a wide frequency range.

Based on the above analysis, the inner relation between the nonlinear vibration absorber and the dynamic response of the system having imbalance-looseness-rub coupled fault is further studied. It can be seen from Figs. 14(a) and (b) that the whirling amplitude of disc sharply decreases in the presence of absorber. This amplitude is only larger than the initial gap at the non-uniform position, and in other cases, it is much smaller than the initial gap. Therefore, the slight partial rub happens

between blades and casing, which causes the pulse-like motion with small amplitude of casing. It is also due to the partial rub that the impact force is expressed in the form of pulse, as shown in Fig. 14(d). To sum up, the absorber could weaken the blade-casing rub in the presence of non-uniform gap, including impact severity and impact frequency.

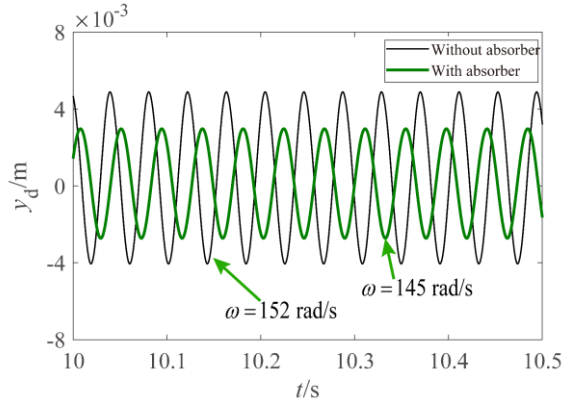

(a) time histories of vertical displacement of disc

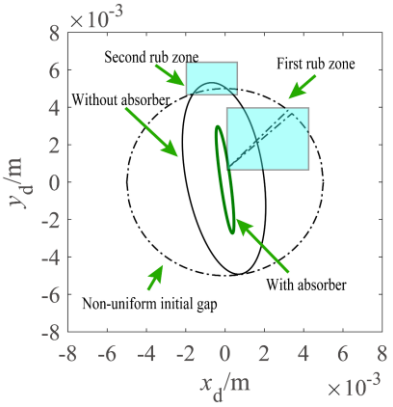

(b) whirling orbit of disc

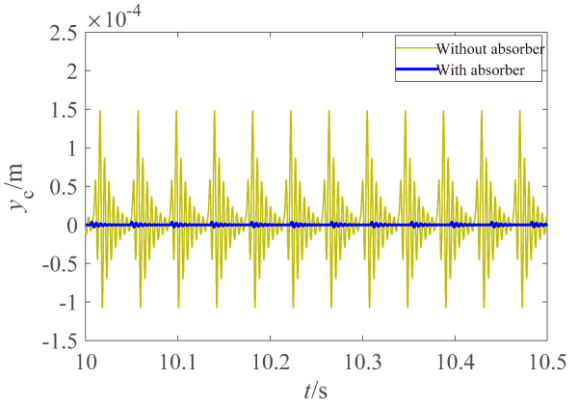

(c) time histories of vertical displacement of casing

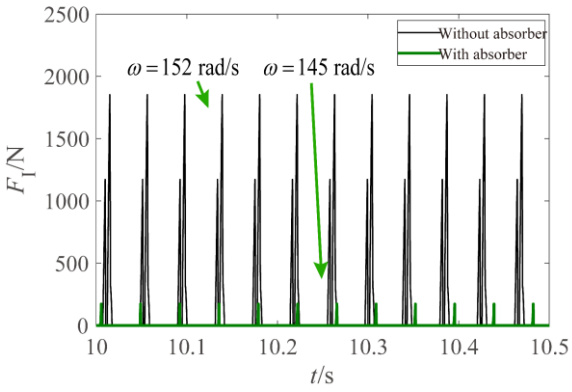

(d) resultant impact force of disc

Fig. 14. Considering nonlinear vibration absorber or not, the dynamic response of the rotor-casing system with imbalance-looseness-rub coupled fault at resonant state: (a) time histories of vertical displacement of disc, (b) whirling orbit of disc, (c) time histories of vertical displacement of casing, and (d) resultant impact force of disc.

The exciting force induced by the mass imbalance is a major source of rotor vibration in field, so it is necessary to analyse the effect of disc eccentricity on the dynamic characteristics of the system with the above coupled fault. In the end, the different disc eccentricities are taken to discuss the change law of vibration response and impact force.

For convenient analysis, two variables η_{k} and η_{m} are defined to describe the different cases of rotational speed and disc eccentricity, namely

$$\begin{cases} e = 5\times10^{-5}\eta_{\mathrm{c}}, \\ \omega = 100+10\left(\eta_{\omega}-1\right), \end{cases} \tag{39}$$

where the ranges of the two variables are set to $\eta_{\mathrm{c}} = \left[5:1:21\right]$ and $\eta_{\mathrm{m}} = \left[1:1:21\right]$, respectively.

Then considering the effect of pedestal looseness, the dynamic characteristics of the system

without and with nonlinear vibration absorber are calculated under the different rotational speeds and disc eccentricities, as shown in Fig. 15. According to the vibration theory, the maximum vibration amplitude of the disc always happens at the resonant rotational speed. Meanwhile, due to the grow of disc eccentricity, the centrifugal force acting on the system tends to increase. So the vertical vibration amplitude of the disc in resonant state increases from 1.68 mm to 8.47 mm.

On this basis, the nonlinear vibration absorber is introduced to the system for reducing the vibration amplitude. With the same growth of disc eccentricity, the vibration amplitude of disc changes from 0.69 mm to 4.97 mm. This illustrates that the absorber can effectively suppress the vibration of the disc, regardless of the level of disc eccentricity. Moreover, considering that the motion of the pedestal and the disc are coupled with each other, it is necessary to discuss the effect of nonlinear vibration absorber on the pedestal vibration. By comparing Fig. 15(c) with Fig. 15(d), it is clear that the nonlinear vibration absorber can reduce the vibration amplitude of pedestal in a wider range of disc eccentricity.

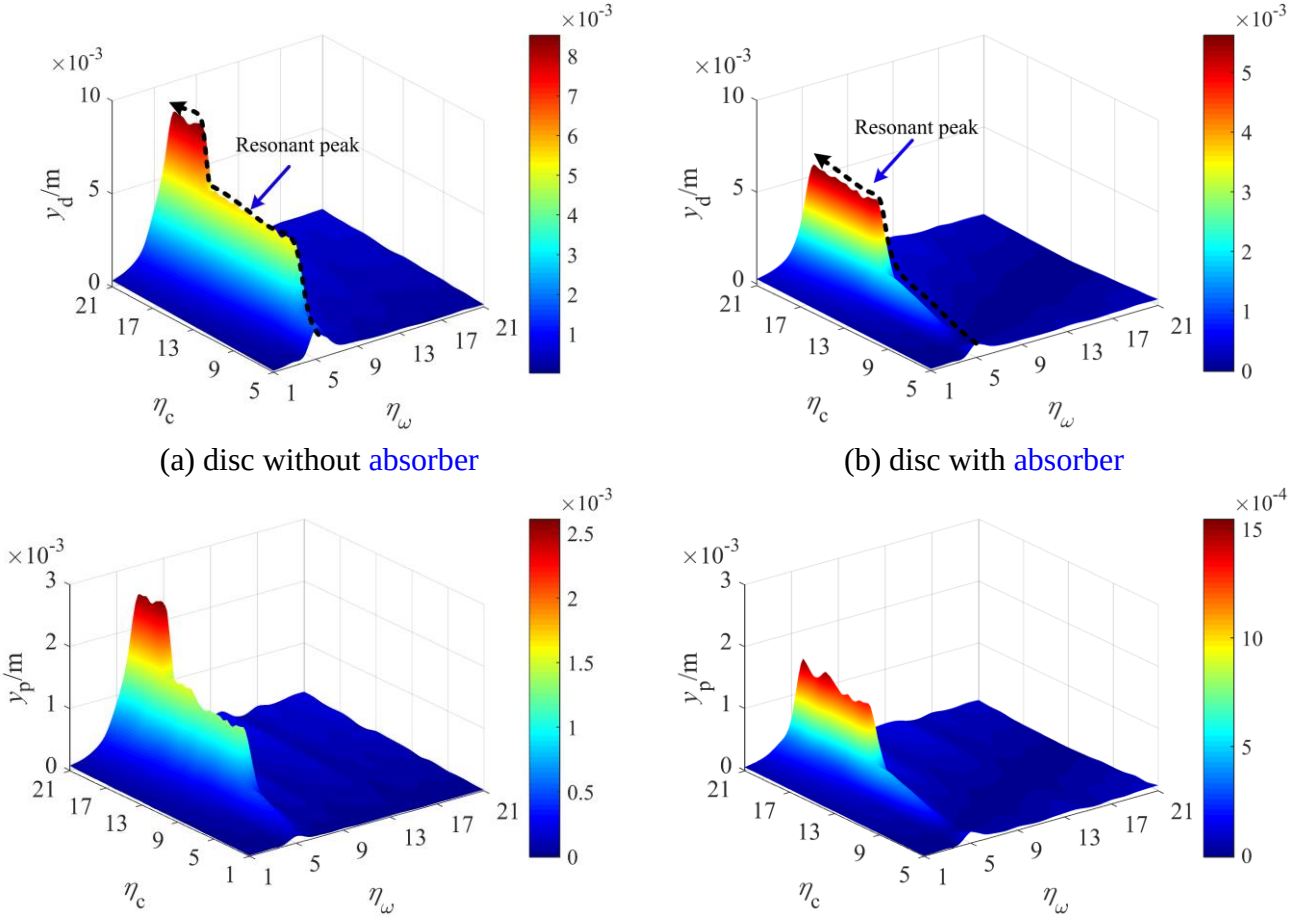

(a) disc without absorber (b) disc with absorber

(c) pedestal without absorber (d) pedestal with absorber

Fig. 15. Vibration displacement of the system having pedestal looseness under different disc eccentricities and rotational speeds: (a) disc without absorber, (b) disc with absorber, (c) pedestal without absorber and (d) pedestal with absorber.

At last, both pedestal looseness and blade-casing rub are taken into account. In the same range of parameters (see Eq. (39)), the effect of nonlinear vibration absorber on the dynamic characteristics of system is further investigated, including rub response and resultant impact force. As shown in Figs.

16(a) and (b), the nonlinear vibration absorber can successfully control the rub response of the disc to a great extent. For example, when the disc eccentricity is 1 mm, the vibration amplitude of the disc is reduced by 31.2%.

What is more, the inner relation between blade-casing rub and absorber is further revealed in the different conditions of rotational speed and disc eccentricity. The whirling amplitude of the disc is an important basis for judging whether rub-impact fault happens. When there is a small eccentricity at the disc, with the contribution of nonlinear vibration absorber, the whirling amplitude of the disc is smaller than the non-uniform initial gap. Under this circumstance, the absorber can prevent the blades and the casing from rubbing. Even if there is a large imbalance happening at the disc, through the absorber, the resultant impact force can decrease from 5558 N to 1959 N.

The above analysis confirms that the nonlinear vibration absorber can suppress the nonlinear vibration of the rotor-casing system with coupled fault under different work conditions. It can also hinder the occurrence of faults to some extent.

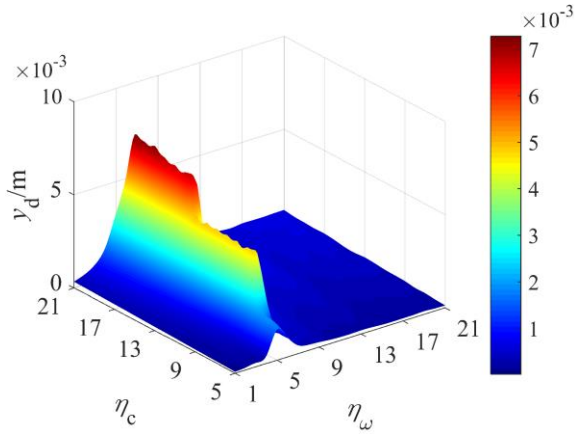

(a) displacement of disc without absorber

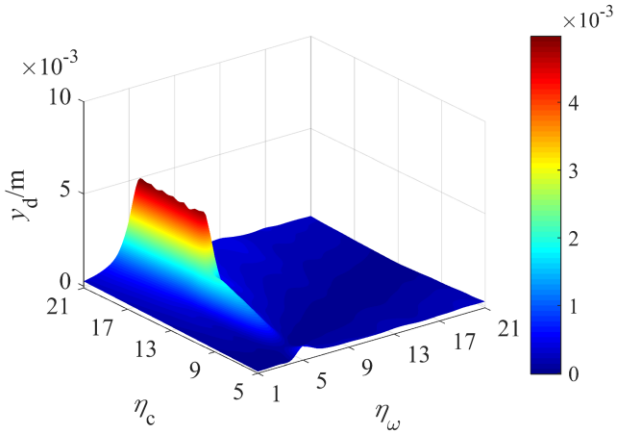

(b) displacement of disc with absorber

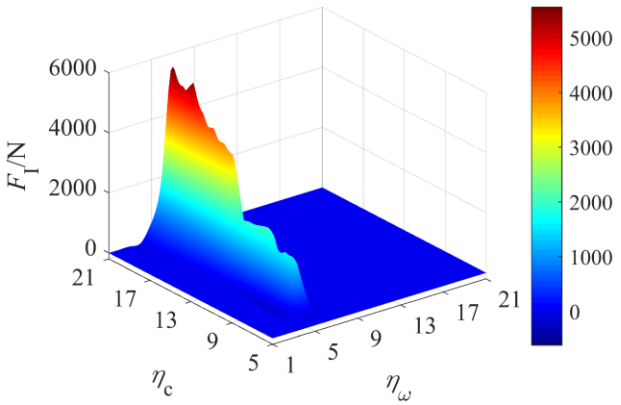

(c) impact force of disc without absorber

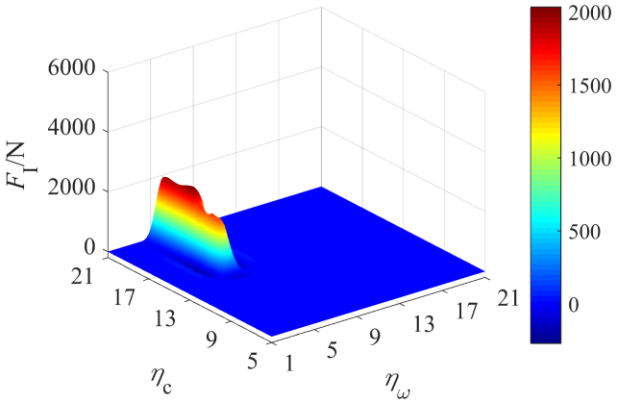

(d) impact force of disc with absorber

Fig. 16. Vibration displacement and resultant impact force of the system having imbalance-looseness-rub coupled fault under different disc eccentricities and rotational speeds: (a) displacement of disc without absorber, (b) displacement of disc with absorber, (c) impact force of disc without absorber, and (d) impact force of disc with absorber.

5. Conclusions

Taking a rotor-casing system having imbalance-looseness-rub coupled fault as the object, a nonlinear vibration absorber is utilized to investigate the vibration mitigation in this paper. By employing the Lagrange's equation, the equations of motion in the presence and absence of the absorber are respectively derived. In the derivation, several key nonlinear factors are considered, such as the geometrical nonlinearity of the shaft caused by whirling motion with large amplitude and the support nonlinearity caused by looseness. For contact analysis, due to the coating inhomogeneity, the initial gap between the blades and the casing is non-uniform rather than ideally uniform. The equations of motion of the system are numerically solved and the dynamic characteristics of the system without and with the absorber are analysed in terms of amplitude-frequency curve, time history of vibration displacement, whirling orbit and colour contour plot. Moreover, the influences of the nonlinear vibration absorber on the blade-casing rub and the pedestal looseness are discussed as well. According to the numerical results, the following conclusions can be obtained.

(1) The nonlinearity of the shaft and the pedestal looseness could directly affect the resonant characteristic of the system. The whirling amplitude of the system is sharply amplified by the pedestal looseness.

(2) The pedestal looseness not only raises the possibility of blade-casing rub, but also aggravates the severity of rub-impact, which is extremely detrimental to the safe operation of rotating machinery.

(3) In a wide frequency range, where the first critical speed is located, the nonlinear vibration absorber can effectively suppress the nonlinear vibration of rotor-casing system. At the same time, the absorber can hinder the possible damage caused by blade-casing rub and pedestal looseness to a great extent.

(4) For different cases of disc eccentricity, the vibration displacement of the system is reduced by the nonlinear vibration absorber. Based on the impact force, the absorber can even prevent the occurrence of rub-impact in some work conditions.

In general, by means of passive control strategy, the complex nonlinear vibration is restrained into regular periodic motion. This is just from the perspective of nonlinear mechanics, which provides a theoretical support for the smooth operation of aero engines.

Acknowledgements

This work was supported by the National Natural Science Foundation of China (Grant No. 11702228, 11772273, 11672052) and the Fundamental Research Funds for the Central Universities (2682017CX087). The first author, Yang Yang, would like to thank the support to his visit to the School of Engineering, University of Liverpool, from the China Scholarship Council (CSC).

Appendix A

Table 1 Main parameters of a rotor-casing system

Physical parameter	Variable	Value
Equivalent mass of disc with blades (kg)	m_d	58.3613

Eccentric mass of disc (kg)	m_e	29.1807
Mass of casing (kg)	m_c	11.6723
Mass of loose pedestal (kg)	m_p	58.3613
Length of shaft (mm)	l	448.8
Radius of shaft (mm)	r	12.2
Elastic modulus of shaft (GPa)	E	210
Structural damping of shaft (N.s/m)	c	261.8
Support stiffness of casing (MN/m)	k_c	20
Support damping of casing (N.s/m)	c_c	2100
Eccentricity of disc (mm)	e	0.5
Radius of disc (mm)	R_d	243.2
Damping of nonlinear vibration absorber (N.s/m)	c_N	26.18
Initial offset of nonlinear vibration absorber (mm)	r_0	12.2
Stiffness of pedestal under the loose state (MN/m)	k_{p1}	10
Damping of pedestal under the loose state (N.s/m)	c_{p1}	350
Stiffness of pedestal under the locked state (MN/m)	k_{p2}	220
Damping of pedestal under the locked state (N.s/m)	c_{p2}	500
Initial loose gap of pedestal (mm)	δ_L	3
Number of blades	N	8
Location of non-uniform gap (rad)	ϕ	$\pi/4$
Range of non-uniform gap (rad)	γ	$\pi/9$
Initial gap between blades and casing (mm)	δ_0	5
Maximum magnitude of non-uniform gap (mm)	δ_{max}	3
Impact stiffness between blades and casing (MN/m)	k_I	1
Coefficient of friction	μ	0.1

References

[1] G.Y. Garoli, H.F.D. Castro, Analysis of a rotor-bearing nonlinear system model considering fluid-induced instability and uncertainties in bearings. J. Sound Vib. 448 (2019): 108-129.

[2] P. Zhou, M.G. Du, S.Q. Chen, Q.B. He, Z.K. Peng, W.M. Zhang, Study on intra-wave frequency modulation phenomenon in detection of rub-impact fault. Mech. Syst. Signal Process. 122

(2019): 342-363.
[3] J.P. Salameh, S. Cauet, E. Etien, A. Sakout, L. Rambault, Gearbox condition monitoring in wind turbines: a review. Mech. Syst. Signal Process. 111 (2018): 251-264.
[4] T.H. Patel, A.K. Darpe, Coupled bending-torsional vibration analysis of rotor with rub and crack. J. Sound Vib. 326 (3-5) (2009): 740-752.
[5] S. Lahriri, H.I. Weber, I.F. Santos, H. Hartmann, Rotor-stator contact dynamics using a non-ideal drive-Theoretical and experimental aspects. J. Sound Vib. 331 (2012): 4518-4536.
[6] M.A. Mokhtar, A.K. Darpe, K. Gupta, Investigations on bending-torsional vibrations of rotor during rotor-stator rub using Lagrange multiplier method. J. Sound Vib. 401 (2017): 94-113.
[7] A.D. Shaw, A.R. Champneys, M.I. Friswell, Normal form analysis of bouncing cycles in isotropic rotor stator contact problems. Int. J. Mech. Sci. 155 (2019): 83-97.
[8] O. Grāpis, V. Tamužs, N.-G. Ohlson, J. Andersons. Overcritical high-speed rotor systems, full annular rub and accident. J. Sound Vib. 290 (3-5) (2006): 910-927.
[9] Y. Yang, D.Q. Cao, T.H. Yu, D.Y. Wang, C.G. Li, Prediction of dynamic characteristics of a dual-rotor system with fixed point rubbing-Theoretical analysis and experimental study. Int. J. Mech. Sci. 115-116 (2016): 253-261.
[10] H. Ma, X.Y. Tai, Q.K. Han, Z.Y. Wu, D. Wang, B.C. Wen, A revised model for rubbing between rotating blade and elastic casing. J. Sound Vib. 337 (2015): 301-320.
[11] X. Dai, X. Zhang, X. Jin, The partial and full rubbing of a flywheel rotor-bearing-stop system. Int. J. Mech. Sci. 43 (2001): 505-519.
[12] G.F. Zhang, W.N. Xu, B. Xu, W. Zhang, Analytical study of nonlinear synchronous full annular rub motion of flexible rotor-stator system and its dynamic stability. Nonlinear Dyn. 57(4) (2009): 579-592.
[13] J.J. Yu, On occurrence of reverse full annular rub. ASME J. Eng. Gas Turbines Power. 134(1) (2011): 012505-1-012505-8.
[14] Y. Choi, Investigation on the whirling motion of full annular rotor rub. J. Sound Vib. 258 (2002): 191-198.
[15] N. Vlajiic, A.R. Champneys, B. Balachandran, Nonlinear dynamics of a Jeffcott with torsional deformations and rotor-stator contact. Int. J. Non-Linear Mech. 92 (2017): 102-110.
[16] N. Vlajic, X.B. Liu, H. Karki, B. Balachandran, Torsional oscillations of a rotor with continuous stator contact. Int. J. Mech. Sci. 83 (2014): 65-75.
[17] P.A. Smyth, P.A. Varney, I. Green, A fractional calculus model of viscoelastic stator supports coupled with elastic rotor-stator rub. ASME J. Tribol. 138(4) (2016): 041101-1-041001-8.
[18] E. Chipato, A.D. Shaw, M.I. Friswell, Frictional effects on the nonlinear dynamics of an overhung rotor. Commun. Nonlinear Sci. Numer. Simul. 78 (2019) 104875-1-12.
[19] P. Pennacchi, N. Bachschmid, E. Tanzi, light and short arc rubs in rotating machines: experimental tests and modelling. Mech. Syst. Signal Process. 23 (2009): 2205-2227.
[20] M. Torkhani, L. May, P. Voinis, Light, medium and heavy partial rubs during speed transients of rotating machines: Numerical simulation and experimental observation. Mech. Syst. Signal Process. 29 (2012): 45-66.

[21] J.-J. Sinou, F. Thouverez, L. Jezequel, Non-linear stability analysis of a complex rotor/stator contact system. J. Sound Vib. 278 (2004): 1095-1129.
[22] T.-N. Ebrahim, A.-S. Pouya, A. Hamid, Nonlinear dynamics of a flexible rotor on tilting pad journal bearings experiencing rub-impact. Nonlinear Dyn. 94 (2018): 2937-2956.
[23] U. Ehehalt, O. Alber, R. Markert, G. Wegener, Experimental observations on rotor-to-stator contact. J. Sound Vib. 446 (2019): 453-467.
[24] Z.Y. Qin, Z.B. Yang, J. Zu, F.L. Chu, Free vibration analysis of rotating cylindrical shells coupled with moderately thick annular plate. Int. J. Mech. Sci. 142-143 (2018): 127-139.
[25] Z.Y. Qin, F.L. Chu, J. Zu, Free vibrations of cylindrical shells with arbitrary boundary conditions: a comparison study. Int. J. Mech. Sci. 133 (2017): 91-99.
[26] L.M. Chen, Z.Y. Qin, F.L. Chu, Dynamic characteristics of rub-impact on rotor system with cylindrical shell. Int. J. Mech. Sci. 133(2017): 51-64.
[27] K. Lu, Y.L. Jin, Y.S. Chen, Q.J. Cao, Z.Y. Zhang, Stability analysis of reduced rotor pedestal looseness fault model. Nonlinear Dyn. 82(4) (2015): 1611-1622.
[28] M. Jiang, J.G. Wu, X.S. Peng, X.J. Li, Nonlinearity measure based assessment method for pedestal looseness of bearing-rotor systems. J. Sound Vib. 411 (2017): 232-246.
[29] Z.Y. Qin, Q.K. Han, F.L. Chu, Bolt loosening at rotating joint interface and its influence on rotor dynamics. Eng. Fail. Anal. 59 (2016): 456-466.
[30] X.J. Jiang, Y.S. Zhu, J. Hong, X. Chen, Y.Y. Zhang, Investigation into the loosening mechanism of bolt in curvic coupling subjected to transverse loading. Eng. Fail. Anal. 32 (2013): 360-373.
[31] A. Muszynska, P. Goldman, Chaotic responses of unbalanced rotor/bearing/stator systems with looseness or rubs. Chaos Solitons Fractals. 5(9) (1995): 1683-1704.
[32] D.S. Alves, M.F. Wu, K.L. Cavalca, Application of gain-scheduled vibration control to nonlinear journal-bearing supported rotor. J. Sound Vib. 442 (2019): 714-737.
[33] C.Z. Guo, M.A. AL-Shudeifat, A.F. Vakakis, L.A. Bergman, D.M. McFarland, Vibration reduction in unbalanced hollow rotor systems with nonlinear energy sinks. Nonlinear Dyn. 79 (2015): 527-538.
[34] Y. Starosvetsky, O.V. Gendelman, Dynamics of a strongly nonlinear vibration absorber coupled to a harmonically excited two-degree-of-freedom system. J. Sound Vib. 312 (2008): 234-256.
[35] S.L. Feudo, C. Touzé, J. Boisson, G. Cumunel, Nonlinear magnetic vibration absorber for passive control of a multi-storey structure. J. Sound Vib. 438 (2018): 33-53.
[36] A.F. Vakakis, O.V. Gendelman, L.A. Bergman, D.M. McFarland, G. Kerschen, Y.S. Lee, Nonlinear targeted energy transfer in mechanical and structural systems. Springer Verlag, 2008.
[37] E. Gourdon, N.A. Alexander, C.A. Taylor, C.H. Lamarque, S. Pernot, Nonlinear energy pumping under transient forcing with strongly nonlinear coupling: Theoretical and experimental results. J. Sound Vib. 300(3-5) (2007): 522-551.
[38] O.V. Gendelman, G. Sigalov, L.I. Manevitch, M. Mane, A.F. Vakakis, L.A. Bergman, Dynamics of an eccentric rotational nonlinear energy sink. J. Appl. Mech.-Trans. ASME, 79 (2012): 011012-1-9.
[39] G. Sigalov, O.V. Gendelman, M.A. AL-Shudeifat, L.I. Manevitch, A.F. Vakakis, L.A. Bergman,

Resonance captures and targeted energy transfers in an inertially-coupled rotational nonlinear energy sink. Nonlinear Dyn. 69(4) (2012): 1693-1704.

[40] Z.N. Ahmadabadi, Nonlinear energy transfer from an engine crankshaft to an essentially nonlinear attachment. J. Sound Vib. 443 (2019): 139-154.

[41] M. Parseh, M. Dardel, M.H. Ghasemi, M.H. Pashaei, Steady state dynamics of a non-linear beam coupled to a non-linear energy sink. Int. J. Non-Linear Mech. 79 (2016): 48-65.

[42] M. Kani, S.E. Khadem, M.H. Pashaei, Vibration control of a nonlinear beam with a nonlinear energy sink. Nonlinear Dyn. 83 (2016): 1-22.

[43] S. Bab, S.E. Khadem, M. Shahgholi, Vibration attenuation of a rotor supported by journal bearings with nonlinear suspensions under mass eccentricity force using nonlinear energy sink. Meccanica, 50 (2015): 2441-2460.

[44] S. Bab, S.E. Khadem, M. Shahgholi, Lateral vibration attenuation of a rotor under mass eccentricity force using non-linear energy sink. Int. J. Non-Linear Mech. 67 (2014): 251-266.

[45] S. Bab, S.E. Khadem, M. Shahgholi, Vibration attenuation of a rotor supported by journal bearings with nonlinear suspensions under mass eccentricity force using nonlinear energy sink. Nonlinear Dyn. 50 (2015): 2441-2460.

[46] G.G. Tehrani, M. Dardel, Vibration mitigation of a flexible bladed rotor dynamic system with passive dynamic absorbers. Commun. Nonlinear Sci. Numer. Simul. 69 (2019): 1-30.

[47] J. Taghipour, M. Dardel, M.H. Pashaei, Vibration mitigation of a nonlinear rotor system with linear and nonlinear vibration absorbers. Mech. Mach. Theory. 128 (2018): 586-615.

[48] T.N. Rhys-Jones, Thermal sprayed coating systems for surface protection and clearance control applications in aero engines. Surf. Coat. Technol. 43/44 (1990): 402-415.

[49] G. Chen, Simulation of casing vibration resulting from blade-casing rubbing and its verifications. J. Sound Vib. 361 (2016): 190-209.

[50] H.F. Wang, G. Chen, P.P. Song, Simulation analysis of casing vibration response and its verification under blade-casing rubbing fault. 138 (2016): 031004-1-14.

[51] H. Ma, X.Y. Zhao, Y.N. Teng, B.C. Wen, Analysis of dynamic characteristics for a rotor system with pedestal looseness. Shock. Vib. 18(1) (2011): 13-27.

[52] Y. Yang, D.Q. Cao, Y.Q. Xu, Rubbing analysis of a nonlinear rotor system with surface coatings. Int. J. Non-Linear Mech. 84 (2016): 105-115.

[53] Y. Yang, Y.R. Yang, D.Q. Cao, G. Chen, Y.L. Jin, Response evaluation of imbalance-rub-pedestal coupling fault on a geometrically nonlinear rotor system. Mech. Syst. Signal Process. 118 (2019): 423-442.

[54] H.L. Yao, Y.B. Cao, Z.Y. Ding, B.C. Wen, Using grounded nonlinear energy sinks to suppress lateral vibration in rotor systems. Mech. Syst. Signal Process. 124 (2019): 237-253.

[55] Y. Starosvetsky, O.V. Gendelman, Interaction of nonlinear energy sink with a two degrees of freedom linear system: Internal resonance. J. Sound Vib. 329 (2010): 1836-1852.